frontiers | Frontiers in Earth Science

TYPE Original Research
PUBLISHED 19 May 2025
DOI 10.3389/feart.2025.1550746

OPEN ACCESS

EDITED BY
Andrea Zanchi,
University of Milano-Bicocca, Italy

REVIEWED BY
Puspendu Saha,
Indian Institute of Technology Kanpur, India
Christian Koeberl,
University of Vienna, Austria
Birger Schmitz,
Lund University, Sweden

*CORRESPONDENCE
Jaime Urrutia-Fucugauchi,
juf@geofisica.unam.mx

RECEIVED 24 December 2024
ACCEPTED 14 April 2025
PUBLISHED 19 May 2025

CITATION
Urrutia-Fucugauchi J, Pérez-Cruz L, Wittmann A, Arz JA, Arenillas I, Xiao L, Zhao J, Gilabert V and Salguero-Hernandez E (2025) Chicxulub central zone structure and stratigraphy—PEMEX exploration drilling program.
Front. Earth Sci. 13:1550746.
doi: 10.3389/feart.2025.1550746

Chicxulub central zone structure and stratigraphy—PEMEX exploration drilling program

Jaime Urrutia-Fucugauchi[1,2]*, Ligia Pérez-Cruz[1,2,3], Axel Wittmann[4], José A. Arz[5], Ignacio Arenillas[5], Long Xiao[6], Jiawei Zhao[6], Vicente Gilabert[7] and Eduardo Salguero-Hernandez[8]

[1]Programa Universitario de Perforaciones en Océanos y Continentes, Instituto de Geofísica, Universidad Nacional Autónoma de México, México, Mexico, [2]Instituto de Investigación Científica y Estudios Avanzados Chicxulub, Parque Científico y Tecnológico de Yucatán, Mérida, Yucatán, Mexico, [3]Coordinación de Plataformas Oceanográficas, Coordinación de la Investigación Científica, Universidad Nacional Autónoma de México, México, Mexico, [4]Eyring Materials Center, Arizona State University, Tempe, AZ, United States, [5]Departamento de Ciencias de la Tierra, and Instituto Universitario de Investigación en Ciencias Ambientales de Aragón, Universidad de Zaragoza, Zaragoza, Spain, [6]State Key Laboratory of Geological Processes and Mineral Resources, School of Earth Sciences, Planetary Science Institute, China University of Geosciences, Wuhan, China, [7]Departament de Dinàmica de la Terra i de l'Oceà, Facultat de Ciències de la Terra, Universitat de Barcelona, Barcelona, Spain, [8]Facultad de Ingeniería, Universidad Autónoma del Carmen, Ciudad del Carmen, Campeche, Mexico

The Chicxulub crater was formed by the impact of an asteroid ~66 Ma ago at the Cretaceous/Paleogene boundary on a carbonate platform in the southern Gulf of Mexico. The impact's structure is not exposed at the surface, requiring drilling and geophysical surveys to study it. The geophysical and drilling program by Petroleos Mexicanos (PEMEX) provided critical evidence and core samples for petrographic, geochemical and chronostratigraphic studies. The PEMEX boreholes drilled through a sequence of carbonate sediments and igneous-textured rocks, corresponding to the post-impact carbonates and impactite sequence. The Chicxulub-1 (1581.5 m), Sacapuc-1 (1527 m), and Yucatan-6 (1645 m) boreholes reached the impact breccias and melt at ~1100–1581.5 m, ~1000–1527 m and 1040/1080–1645 m, respectively. In the Chicxulub-1 and Sacapuc-1 boreholes, post-impact sediments include interbedded marlstones and limestones, and in Yucatan-6, post-impact sediments include limestones, with intercalated layers of marlstones, calcarenites and calcirudists, and a sandy unit between 1040/1080 and 1220/1250 m, interpreted as a carbonate-rich sorted suevite. The impactites are ~300 m and ~200 m thick in Sacapuc-1 and Chicxulub-1 boreholes, respectively. Lateral correlations document that the melt sheet/pockets extend across the annular trough and peak ring. Self-potential (SP) logs characterize the carbonate and impactite sections that can be traced across the central zone, with differences in depth and thickness. SP logs record the carbonate and impactite section stratigraphy, with units that can be traced across the central zone. Lithological changes are observed at a depth below ~900 m in the impactite section. The PEMEX drilling ended within the impactite section, without reaching the target carbonates. The revised borehole columns, logs, micropaleontological reports, and geophysical models provide constraints on

post-impact sediments and impactites across the peak ring and annular trough in the central zone.

KEYWORDS

Chicxulub impact structure, drilling, logging, stratigraphy, impact breccia, melt

1 Introduction

The Chicxulub structure was formed ~66 Ma ago by the impact of an asteroid on the Yucatan platform in the southern Gulf of Mexico (Hildebrand et al., 1991; Schulte et al., 2010). After formation, carbonate deposition continued, covering the structure, which is now located part offshore and part on land, with its geometric center on the coastline (Figure 1). The Petroleos Mexicanos (PEMEX) oil exploration program launched in the 1940s documented a regional amplitude gravity anomaly in northwestern Yucatan (Cornejo-Toledo and Hernandez-Osuna, 1950). It was subsequently investigated by drilling, and an igneous-textured unit of andesitic composition was found beneath the carbonate sediments at ~1 km depth. Aeromagnetic surveys in the late 1970s revealed high-amplitude dipolar magnetic anomalies within the regional gravity anomaly, which were interpreted in terms of a large impact structure by Penfield and Camargo-Zanoguera (1981).

Studies linked the Chicxulub impact to the End-Cretaceous mass extinction at the Cretaceous/Paleogene (K/Pg) boundary (Alvarez et al., 1980; Hildebrand et al., 1991; Schulte et al., 2010). After formation, the structure was covered by carbonate sediments, and at present, there are no outcrops of the structure and ejecta deposits in the nearby areas. Studies depend on geophysical surveys, drilling, and theoretical and numerical models. The PEMEX data proved crucial for characterizing the structure and its stratigraphic positioning based on the impactites and pre- and post-impact carbonate sequences. The boreholes investigated the central zone within the gravity and magnetic anomalies, sampling the impact breccias and melt rocks (Hildebrand et al., 1998; Sharpton et al., 1992). Initial analyses raised questions on the structure and stratigraphy, which included age assignments from lateral correlations and planktic foraminifera biostratigraphy, with the age of the igneous-textured unit assigned to the late Cretaceous (López Ramos, 1975; López Ramos, 1983; Ward et al., 1995). The late Cretaceous era presented problems to associate the impact with the K/Pg boundary impact. Tackling these questions and the validation of the impact theory proposed by Alvarez et al. (1980) was limited by the partial access to PEMEX original reports, logs, and core samples.

Chicxulub impact structure has been explored in drilling programs, resulting in continuous core recovery (Figure 2). The Chicxulub Drilling Program including eight boreholes in the central and southern sectors that drilled into the carbonate and impactite sequences providing continuous core samples is one such example (Urrutia-Fucugauchi et al., 1996). The Chicxulub Scientific Drilling Project by the International Continental Drilling Program (ICDP) and UNAM carried out drilling of the Yaxcopoil-1 borehole in the terrace zone, southern terrace sector (Urrutia-Fucugauchi et al., 2004). The Federal Commission of Electricity (CFE)-UNAM drilled three boreholes in the eastern Valladolid sector (Urrutia-Fucugauchi et al., 2008). The peak ring in the marine central sector was drilled as part of the International Ocean Discovery Program (IODP)-ICDP Expedition 364 M0077A borehole (Morgan et al., 2016; Morgan et al., 2017).

In this study, we review and analyze unpublished data, geophysical logs, and core samples of the Chicxulub-1, Sacapuc-1, and Yucatan-6. Analysis provides revised borehole columns, logs, and correlations, which constrain the stratigraphy of post-impact carbonates and impact breccias and melt. It provides an update of the planktic foraminiferal record and the age of impact breccias and post-impact sediments in the PEMEX boreholes.

2 Chicxulub

The structure, located in northwestern Yucatan, southern Gulf of Mexico, has a rim diameter of ~200 km with a multiring and peak ring morphology. The rim is expressed at the surface by the ring of cenotes and a topographic depression, associated with differential subsidence of the interior zone and radial fault system.

Following the proposal by Hildebrand et al. (1991) that Chicxulub impact was caused by Cretaceous–Paleogene (K/Pg) events, PEMEX cores were re-analyzed, with radiometric dates confirming the K/Pg age (Sharpton et al., 1992). The impact occurred during the Chron 29r, shown by reverse polarity in the melt and breccia samples and the inverse dipolar magnetic anomaly (Urrutia-Fucugauchi et al., 1994; Pilkington et al., 1994; Rebolledo-Vieyra and Urrutia-Fucugauchi, 2006). Studies showed that the globally distributed distal ejecta deposits correlated with the K/Pg boundary, with distribution of shocked quartz and other mineralogical impact markers indicating a single source, coincident with the Chicxulub impact site (Alvarez et al., 1995; Claeys et al., 2002; Morgan et al., 2006; Molina et al., 2006; Arenillas et al., 2006; Kuiper et al., 2008), and radiometric dates on impact-metamorphosed zircons from K/Pg boundary sections supporting a genetic relationship with the Chicxulub impact (Krogh et al., 1993; Kamo et al., 2011).

Seismic reflection surveys have been carried out by PEMEX and later as part of the 1996 British Institutions Reflection Profiling Syndicate (BIRPS) survey and the 2005 Chicxulub Seismic Experiment (Morgan et al., 1997; Gulick et al., 2008). The BIRPS survey included regional profiles trending E–W across the platform, while the Chicxulub Seismic Experiment focused on the central sector. Joint analyses of the seismic surveys, borehole information, and geophysical logs characterize the structure, stratigraphy, and petrophysics (Hildebrand et al., 1998; Bell et al., 2004; Urrutia-Fucugauchi et al., 2011; Urrutia-Fucugauchi et al., 2025; Gulick et al., 2013).

Geophysical surveys image the basin, terrace zone, rim, target carbonate sequence and deep crustal basement (Figure 3). Post-impact carbonate sediments fill the basin and surrounding area in the carbonate platform, with the basin floor marked by high-energy

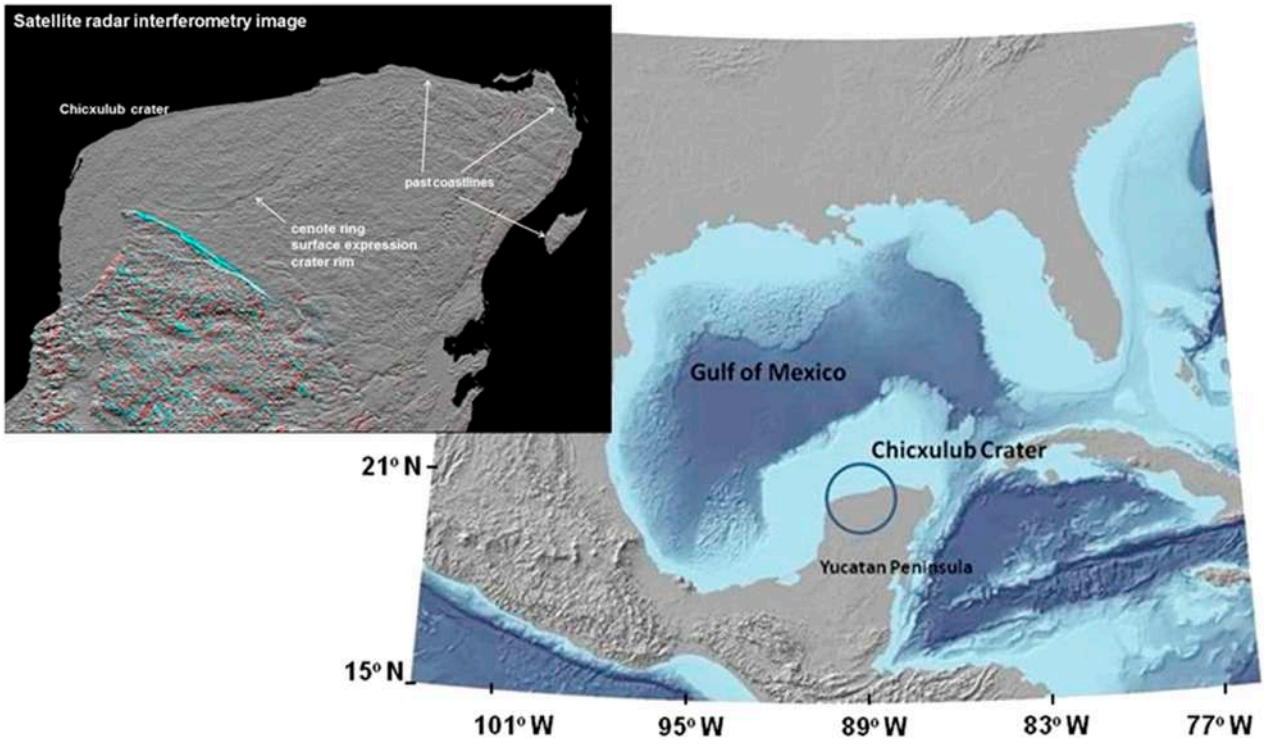

FIGURE 1
Chicxulub location in the southern Gulf of Mexico (base map after French and Schenk, 2004). Chicxulub has a rim diameter of ~200 km, located on the northern Yucatan peninsula, with an approximate center along the coastline at Chicxulub Puerto. Inset: Satellite radar interferometry image of the Yucatan peninsula (credit NASA Jet Propulsion Laboratory). The buried structure is marked on the surface by a semicircular ring of cenotes and topographic depression. Shown are past coastlines and Ticul fault (Urrutia-Fucugauchi et al., 2008).

reflectors with the contact between the basal Paleocene sediments and impact breccias. Impact produced a major disturbance in the Gulf of Mexico–Caribbean Sea and surrounding areas, generating tsunamis and high energy flows (Goto et al., 2004). The basin floor reflectors delineate the bathymetric peak ring structure. Dipping inward reflectors mark the terrace zone, with normal faulted blocks. The asymmetries are also shown in the potential field models, which have been related to the impact angle and trajectory or to pre-existing characteristics in the target zone (Hildebrand et al., 1998; Pilkington and Hildebrand, 2000; Gulick et al., 2008; Collins et al., 2008; Collins et al., 2020; Urrutia-Fucugauchi et al., 2022).

Morgan et al. (2000) reported tomographic images in the central sector across the peak ring and annular trough, which delineate sub-horizontal and dipping reflectors and low- and high-velocity zones. The low velocities (~3.8 km/s; Morgan et al., 2000) were associated to an upper impact breccia unit, drilled in the Chicxulub-1, Sacapuc-1, and Yucatan-6 boreholes, which suggests it extends across the peak ring into the annular trough. The peak ring appears as a structural discontinuity with distinct lithologies of uplifted deeply shocked basement on top of downthrown weakly shocked collapsed rocks (Morgan et al., 2000; Morgan et al., 2016; Christeson et al., 2018 Chirsteson et al., 2021). Dipping reflectors beneath the peak ring are marked by an abrupt decrease in seismic velocities and the high velocities associated with melt rocks, which are found at ~1.4 km in the Chicxulub-1 and Sacapuc-1 boreholes, and in the annular trough in the Yucatan-6 borehole.

Gulick et al. (2013) interpreted the coherent melt sheet to the sector, as limited by the peak ring, with discrete melt pockets distributed in the annular trough. By analyzing the seismic reflection profiles, they estimate a depth to the top of the melt sheet of approximately 2 km. The thickness is not well constrained. An upper bound estimate of ~3 km was made, taking into consideration previous estimates of the melt volume and the areal extent of the central zone inside the peak ring (Barton et al., 2010). This places the bottom of the melt sheet above the central uplift, as modeled using seismic and gravity data (Vermeesch and Morgan, 2008; Vermeesch et al., 2009).

Seismic attributes increasingly applied in the oil industry are useful to enhance selected properties in seismic profiles and seismic cubes (Taner et al., 1979; Chopra and Marfurt, 2005; Chopra and Marfurt, 2008). Salguero-Hernández et al. (2010) and Salguero-Hernández et al. (2020) reported results of an analysis of seismic attributes for the BIRPS seismic lines, providing petrophysical characterization data of the carbonate and impactite units. For this study, further analysis is done with post-stack seismic traces transformed into complex trace attributes for petrophysics and structural/stratigraphic mapping of layer thickness, geometry, facies changes, and discontinuities.

Integration of oil exploration data and recent surveys offers further insights into the structure and stratigraphy, also highlighting uncertainties and challenges associated with modeling and interpretation (Melosh, 1989; Melosh and Ivanov, 1999; Pierazzo

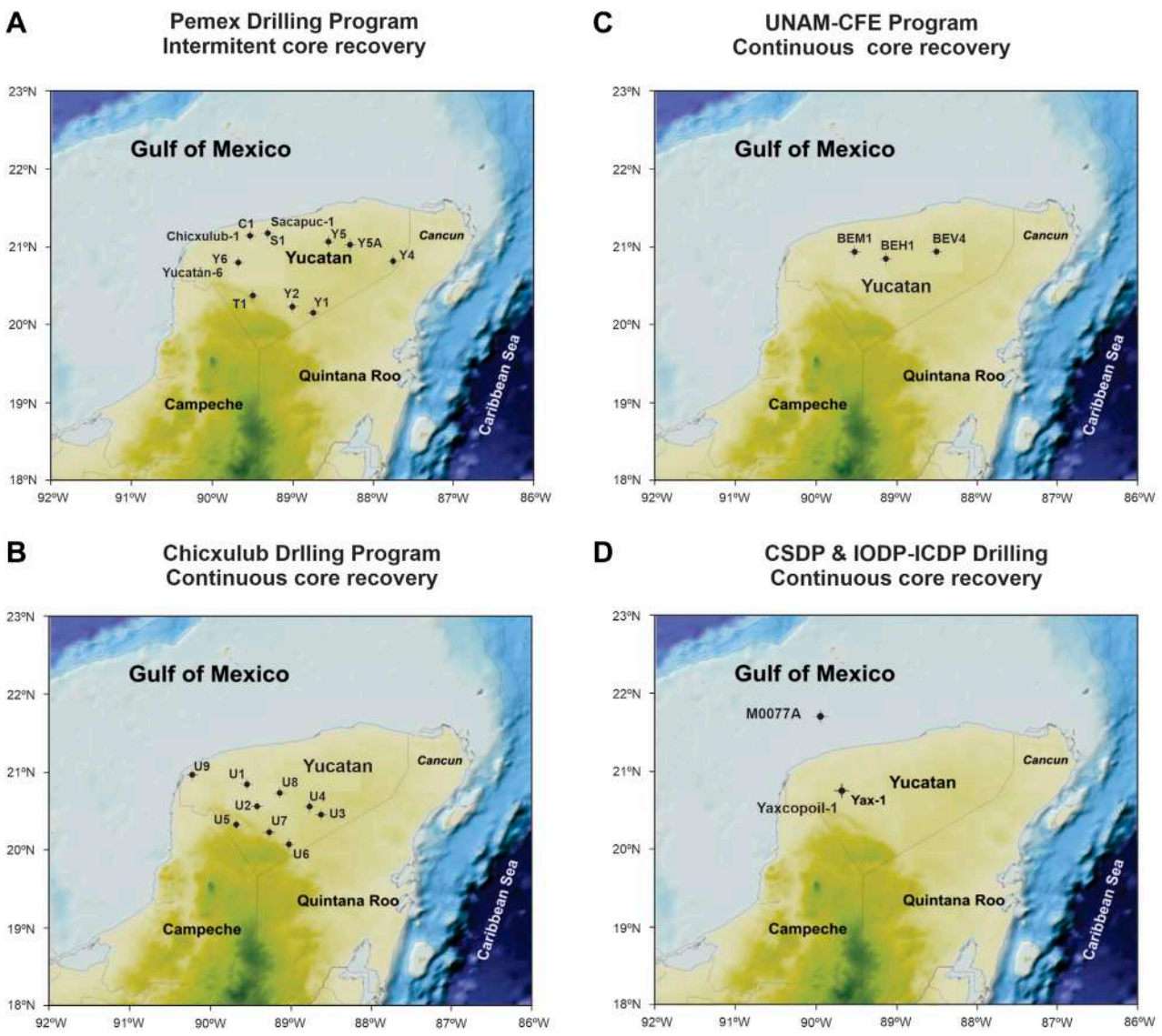

FIGURE 2
Location of drilling sites in the Yucatan peninsula. **(A)** PEMEX oil drilling program. **(B)** Chicxulub drilling program. **(C)** ICDP-UNAM drilling project and IODP-ICDP Chicxulub Expedition. **(D)** UNAM-CFE drilling project (modified from Urrutia-Fucugauchi et al., 2011).

and Melosh, 2000; Collins et al., 2008; Collins et al., 2020; Gulick et al., 2013; Duong et al., 2023; Pérez-Cruz and Urrutia-Fucugauchi, 2024). Difficulties include imaging the melt sheet and central basement uplift from the seismic reflection data, defining the extent of melt sheet and breccia units, characterizing the low-velocity zone beneath the peak ring and annular trough, and faulting and structural asymmetries (Barton et al., 2010; Christeson et al., 2021).

3 PEMEX exploration program

The geophysical surveys documented a regional gravity anomaly in the northern sector of the Yucatan peninsula, which was investigated in the Chicxulub-1 borehole. The drilling program continued, with the Ticul-1 and Sacapuc-1 boreholes, and eventually comprised nine boreholes in the area (Figure 2A; Supplementary Appendix A1). The logging program included caliper, resistivity, self-potential, gamma ray, dip, and hydrocarbon logs, which were acquired from the surface to the final depth. The oil exploration borehole data, lateral correlations, and micropaleontological analyses were used for reconstructing the subsurface stratigraphy, assigning the igneous-textured unit to the upper Cretaceous (Turonian?) beneath the sedimentary sequences belonging to the Maastrichtian to Pliocene ages (López Ramos, 1975; López Ramos, 1983).

Contrasting interpretations about impact age and stratigraphy were proposed. Meyerhoff et al. (1994) interpreted the structure as a Late Cretaceous volcanic center. Ward et al. (1995) concluded that the structure was formed by an impact in the Late Cretaceous, considering more than one episode of brecciation and assuming the breccias were overlain by a ~18-m marl uppermost Maastrichtian

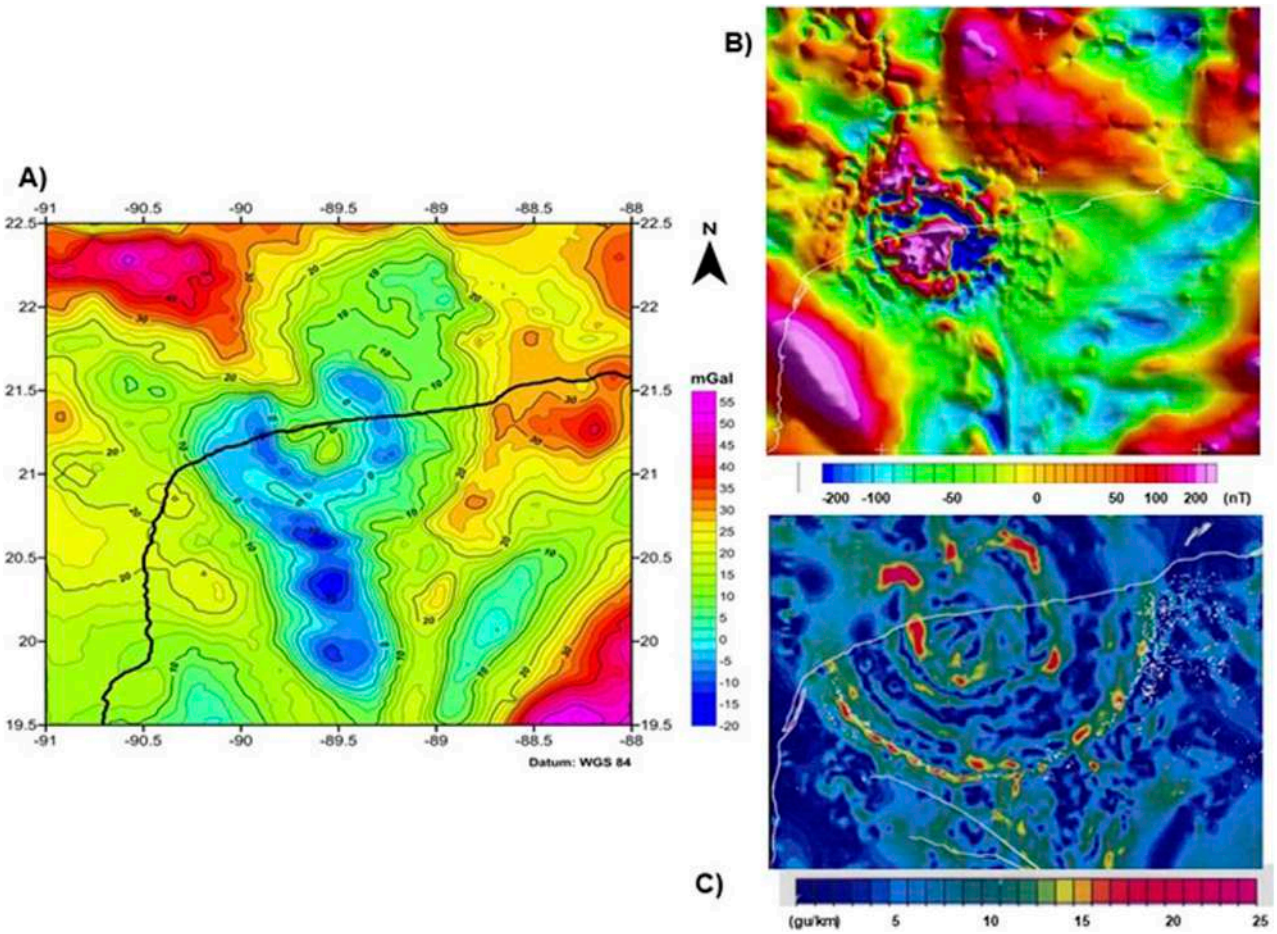

FIGURE 3
Chicxulub gravity and magnetic anomalies. **(A)** Bouguer gravity anomaly (Sharpton et al., 1993; Gulick et al., 2013, 2017). **(B)** Aeromagnetic anomaly (Pilkington and Hildebrand, 2000). **(C)** Horizontal gradient of the gravity field (Connors et al., 1996).

unit (Marín et al., 1994). The top of the breccias in the Chicxulub-1 borehole was identified at 938 m, and the top of the Cretaceous at 920 m. Ward et al. (1995) mentioned that the above studies had drawbacks such as follows: except for two breccia samples from Yucatan-6, no samples from Chicxulub-1, Sacapuc-1, Yucatan-6, and Ticul-1 boreholes were analyzed.

Initial interpretations derived from the drilling and gravity and magnetic anomaly models came to different estimates of the size and morphology, with diameters ranging from less than 180 km up to 300 km (Hildebrand et al., 1991; Hildebrand et al., 1998; Sharpton et al., 1993; Pilkington et al., 1994; Ward et al., 1995).

3.1 PEMEX boreholes

The information includes the following: (a) reports on the drilling advance, cuttings and core descriptions, petrography, and logging; (b) reports on the petrography and biostratigraphy for the core samples and cuttings; (c) final reports for each drilling project (Petroleos Mexicanos, 1953; Petroleos Mexicanos, 1955; Petroleos Mexicanos, 1967). For this study, we concentrate on the Chicxulub-1, Sacapuc-1, and Yucatan-6 boreholes, which sampled the impactite units in the central zone. Drilling incorporated downhole logging and intermittent core recovery. The descriptions from the reports of the lithological columns and the intervals cored are summarized below (see Supplementary Appendices A1–A4).

3.1.1 Chicxulub-1 borehole

Chicxulub-1 was drilled between June and December 1952. The drilling site was selected to investigate the underground structure beneath a large regional gravity anomaly. The drilling site is located at the Chicxulub Pueblo village, with the following coordinates: 21.125 N, 89.5283 W (Figure 2). The final drilling depth was 1581.5 m.

Descriptions of the lithostratigraphic column for the Chicxulub-1 borehole are summarized as follows (Petroleos Mexicanos, 1953; Limon and Baron, 1954; Pérez-Drago et al., 2008; Supplementary Appendix A2). Units were assigned to the following: undifferentiated (0–253 m), Lower Miocene (253–305 m), Upper Oligocene (305–415 m), Middle Oligocene (415–455 m), Lower Oligocene (455–505 m), Upper Eocene (505–590 m), Middle Eocene (590–680 m), Lower Eocene (680–805 m), Paleocene (805–910 m), Upper Cretaceous (910–1275 m), and the igneous-textured unit (1275–1581.5 m).

Ten intervals were cored from 250 to 1394 m, with low recovery rates observed, except for the deepest interval C1–N10. The section from surface to 910 m is formed by interbedded limestones and marlstones. C1–N1 250–253 m, no recovery; C1–N2 253–256 m, argillaceous marl; C1–N3 275–278 m, argillaceous marl; C1–N4 297–300 m, no recovery; C1–N5 300–303 m, argillaceous marl; C1–N6 1299–1300 m, green-black andesitic glass fragment; C1–N7 1300–1301 m, green-black andesitic glass fragment; C1–N8 1301–1303 m, green-black andesitic glass fragment; C1–N9 1390–1393 m, microcrystalline igneous-textured rock with plagioclase, pyroxene and augite crystals, and andesitic composition; C1–N10 1393–1394 m, microcrystalline igneous-textured rock.

3.1.2 Sacapuc-1 borehole

Sacapuc-1 was drilled between March and June, 1954. The drilling site was determined from analyses of the gravity high and geological data, within the residual anomaly possibly associated with a larger regional structure. The drilling site was located at the Motul village with the following coordinates: 21.1428 N, 89.3397 W (Figure 2A). The final drilling depth was 1527 m. The PEMEX report is summarized below and in Supplementary Appendix A3.

In the initial description, units were as follows: Pleistocene carbonates (0–235 m), Miocene carbonates (235–415 m), Oligocene argillaceous limestones (415–570 m), Eocene fine-grained limestones (570–925 m), and Upper Cretaceous carbonates and igneous-textured unit (925–1430–1527 m). The bottom section was described as a black-to-black gray hard andesitic glassy unit.

The lithological column correlates with the nearby Chicxulub-1 well, located approximately 18 km to the SW. Lithological variations are more notable beneath 900 m, where the PEMEX report describes a 400-m sequence of breccias compared to the 200-m sequence documented in Chicxulub-1. The top of the igneous textured unit was cut at 1430 m, whereas in Chicxulub-1, it was cut at 1270 m.

Petrographic descriptions are available for cuttings and core samples (Supplementary Appendix A3). In this regard, the drilling report mentions that cuttings from 0 to 300 m interval were mixed (contaminated). Intermittent core recovery resulted in 20 intervals sampled distributed downcore from 409 to 1474 m. Core analysis permits to constrain the lithologies for the post-impact sequence (0–925 m) and the impactite units (925–1527 m).

The post-impact sediments extend from the surface down to 925 m and were sampled at the following: S1–N1 409–413 m, limestones, argillaceous limestone, and marlstones; S1–N2 439.1–440.6 m, limestones and marlstones; S1–N3 564–567 m ochre marlstones; S1–N4 633.7–636.7 m, fine-grained limestones; S1–N5 636.7–640.7 m, limestones; S1–N6 700–703 m, limestones; S1–N7 755.5–758.5 m, limestones; S1–N8 820–823 m, limestones; S1–N9 858–861 m, limestones; S1–N10 900–903 m, grey-greenish limestones and argillaceous limestones. The section from 925 to 1430 m corresponds to reworked sediments and the impact breccias, sampled at S1–N11 999.2–1002 m, carbonate breccias; S1–N12 1002.2–1005.2 m, carbonate breccias with glassy fragments and anhydrite; S1–N13 1016.7–1021.7 m, bentonitic breccias; S1–N14 1021.7–1024.2 m, bentonitic breccias; SN15 1067.2–1070.8 m, green bentonitic breccias with carbonate clasts, S1–N16 1174–1177 m, green breccias with dark gray limestone clasts and glassy melt particles; S1–N17 1246–1249 m, dark gray limestone; S1–N18 1365–1368 m, carbonate breccias. The melt unit extends from 1430 to 1527 m and is sampled at S1–N19 1438–1439.4 m, glassy black igneous-textured rocks, and S1–N20 1472.5–1474.3 m, igneous-textured rock with thin gray-brown intercalated limestones.

3.1.3 Yucatan-6 borehole

Yucatan-6 was drilled between September 23 and 28 December 1966. The drilling site was determined from analyses of previous drilling, geophysical modeling of gravity anomalies, and surface geological data. The Yucatan-6 borehole is located west of the Chicxulub-1 and Sacapuc-1 boreholes, within high gravity anomaly. The drilling site is located 3 km SW of Uman village, with the following coordinates: 20.8572 N, 89.7542 W (Figure 2A). The total depth was 1645 m.

Descriptions of lithostratigraphic column for the Yucatan-6 borehole are summarized in Supplementary Appendix A4, with units assigned to the following: Miocene white limestones (0–90 m), Oligocene carbonates (90–440 m) with limestones, calcarenites, calcareous lutites, and marlstones, Middle Eocene limestones (440–750 m), Paleocene limestones (750–1000 m), Upper Cretaceous sandy unit with limestones, bentonite breccias, and green-gray sandstones (1000–1259 m), and Upper Cretaceous igneous-textured unit (1259–1645 m). The unit is a black-to-black-gray hard andesitic glassy rock with intervals of bentonitic breccias, anhydrites, and limestones.

Twenty-two intervals at different depths were cored, sampling different lithologies: Y6–N1 107–110 m white limestones; Y6–N2 160–163 m calcareous lutites-marls; Y6–N3 220–223 m calcareous lutites-marls; Y6–N4 304–307 m calcareous lutites-marls; Y6–N5 400–403 m limestones; Y6–N6 447–450 m limestones; Y6–N7 502–505 m limestones; Y6–N8 600–603 m white limestones; Y6–N9 700–703 m limestones; Y6–N10 801.35–802.35 m no recovery; Y6–N11 888–891 m no recovery; Y6–N12 1000–1003 m white limestones; Y6–N13 1200–1203 m green gray sandy unit; Y6–N14 1208–1211 m green bentonitic carbonate breccias; Y6–N15 1253–1256 m green bentonitic silicious breccias; Y6–N16 1293–1295 m igneous-textured rock; Y6–N17 1295.5–1299 m igneous-textured rock; Y6–N18 1351–1354 m igneous-textured rock; Y6–N19 1377–1379.5 m igneous-textured rock; Y6–N20 1506.1–1509.1 m igneous-textured rock; Y6–N21 1586–1591 m andesitic bentonitic breccias; and Y6–N22 1642–1645 m andesites and anhydrites.

4 Methods and results

We analyze the lithostratigraphic columns and lateral correlations from the PEMEX drilling reports, digitized borehole logs, core samples, and geophysical models. The self-potential (SP) logs were digitized from the log printouts and correlated to the lithological columns. Analysis of the SP logs permits to characterize the carbonate sediments and the impactites, which present distinct waveforms and downcore patterns. The revised lithological columns and the SP logs for the Chicxulub-1, Sacapuc-1, and Yucatan-6 boreholes are shown in Figures 4–6, respectively.

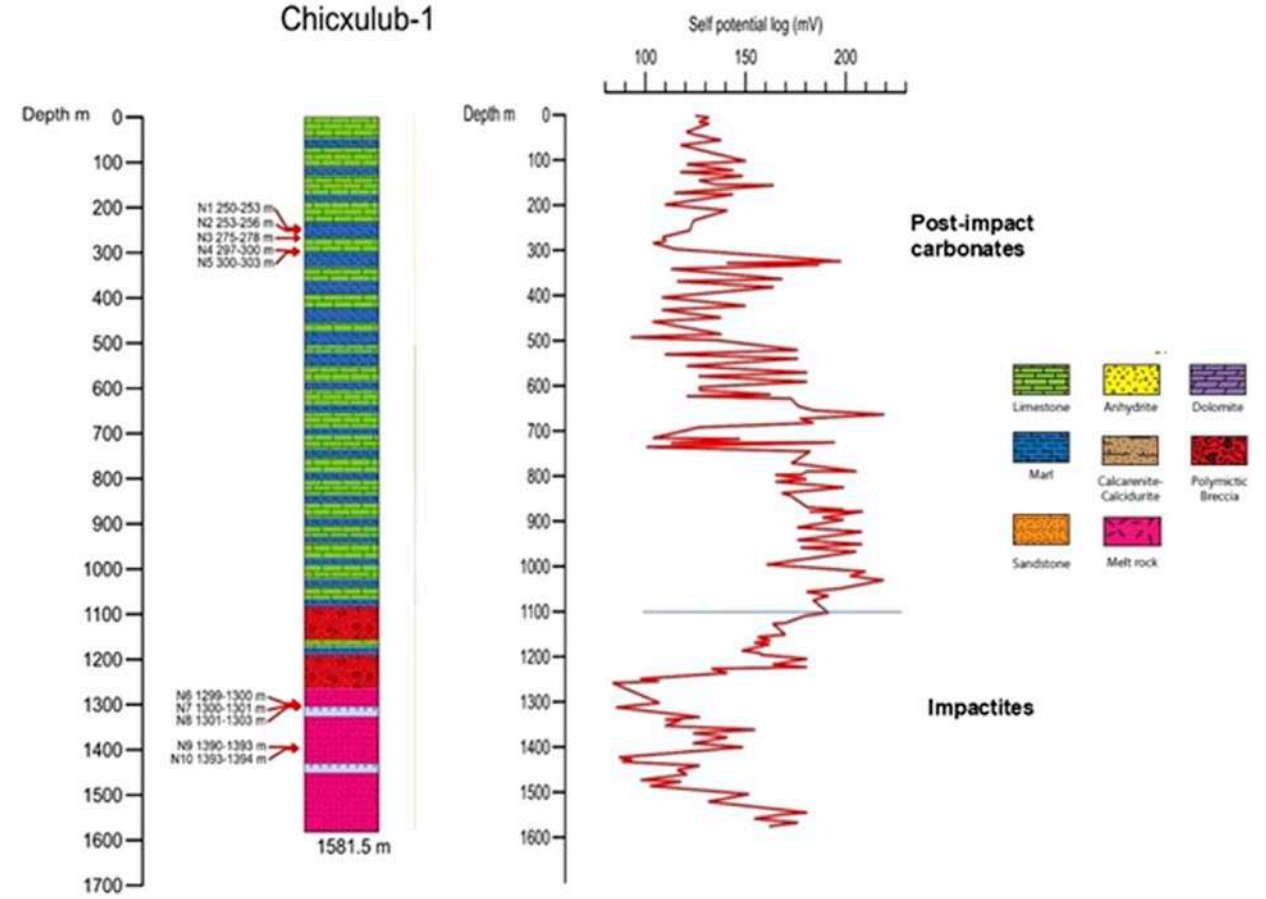

FIGURE 4
Lithological column and self-potential log for the Chicxulub-1 borehole (see Figure 2A for the location of the drilling site and Supplementary Appendix A2 for information on depths and description of cored intervals). The contact between the post-impact carbonates and impactites is marked by the horizontal line.

4.1 Petrography and geochemistry

The PEMEX intermittent coring program provided samples for petrographic, chemical, and petrophysical analyses, but only at given intervals spaced down the column. Analyses have focused on the carbonate–impactite contact and melt and melt-rich breccia units, which are characterized by several subunits with intercalated breccias and carbonate layers. Core images for the Chicxulub-1 and Yucatan-6 boreholes are shown in Figure 7.

For the Chicxulub-1 borehole, contact with the impactite unit lies at approximately 1080 m. The impactite section from 1080 to 1581.5 m is characterized by lower-frequency fluctuations. The upper part from 1080 to 1190 m is characterized by a broad minimum that corresponds to the sorted suevites, with intercalated marlstones (1170–1190 m). At a depth below 1275 m, the SP log shows a step increase forming the second broad minimum, with the interval from 1275 to 1581.5 m corresponding to the melt-rich unit. The SP log shows high-frequency fluctuations superimposed on a low-frequency trend in the upper section of the post-impact carbonates characterized by interbedded limestones and marlstones (Figure 4).

In the Yucatan-6 borehole, analysis for the igneous-textured rocks confirmed the occurrence of shock deformation features and a K/Pg age (Kring and Boynton, 1992; Sharpton et al., 1992). Kring and Boynton (1992) described the augite-bearing rock, characterized by microcrystalline groundmasses of augite, alkali, and plagioclase feldspars with minor contents of magnetite, ulvospinels, and apatite. Augite and feldspar coronas surround quartz xenoliths, which have been reported in impact melt sheets, such as in the Manicouagan crater (Simonds et al., 1978). Anhydrite and quartz veins and cavity fillings point to hydrothermal alterations and associations with the evaporites within the Yucatan target sediments. The augite-bearing melt and Haitian K/Pg glasses show compositions along a mixing trend. Schuraytz et al. (1994) described the Y6–N17 and Y6–N19 intervals as melt-rich matrix suevites with angular to sub-rounded melt clasts. Petrographic and whole-rock and trace geochemical analyses for the Yucatan-6 and Chicxulub-1 cores were reported by Warren et al. (1996), Kettrup et al. (2000) and Claeys et al. (2003).

Dominant clast types resemble the matrix, which shows "subhedral to euhedral pyroxenes and plagioclases in a cryptocrystalline quartz felspathic mesostasis." Minor minerals are

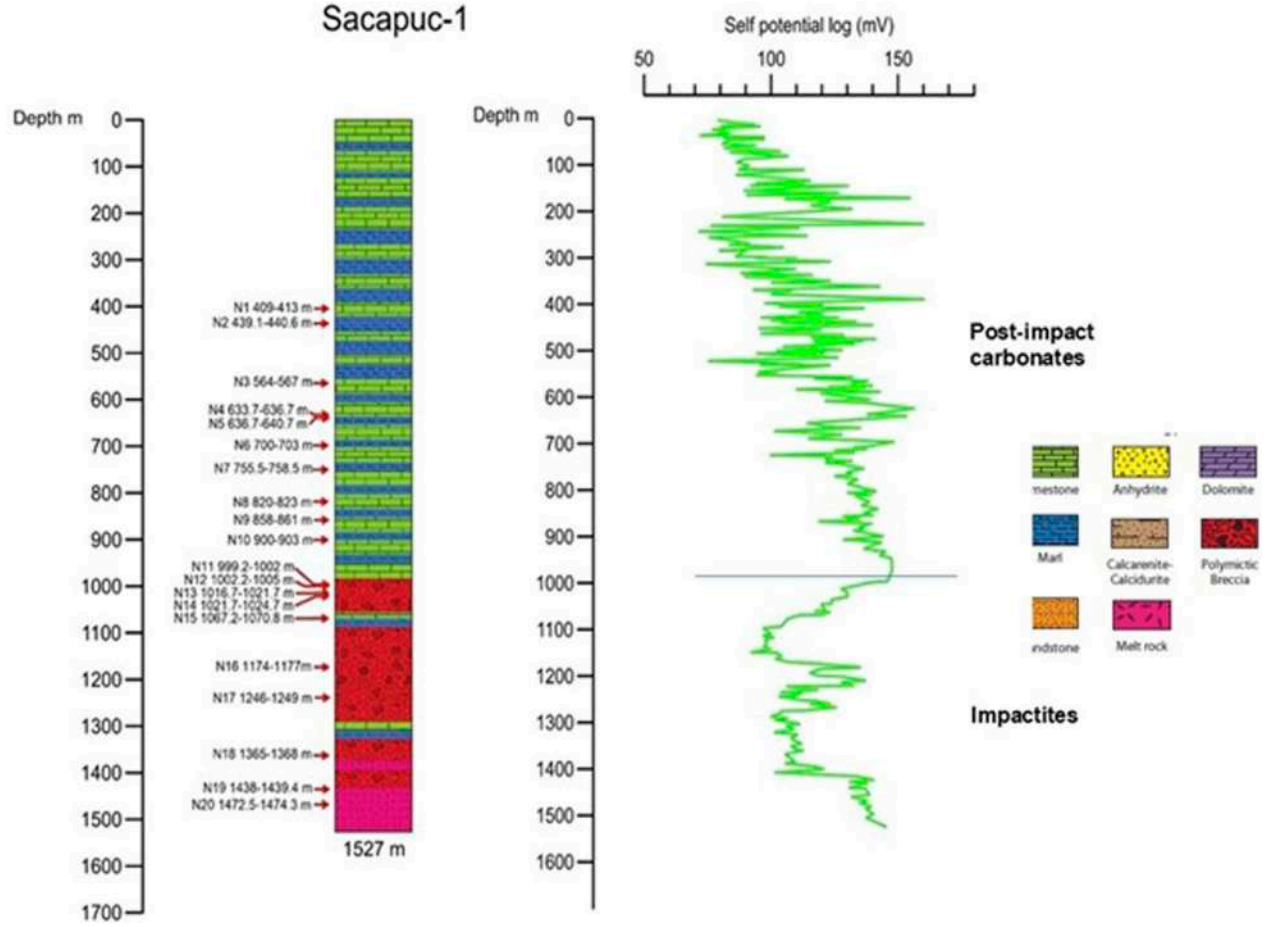

FIGURE 5
Lithological column and self-potential log for the Sacapuc-1 borehole (see Figure 2A for the location of the drilling site and Supplementary Appendix A3 for information on the depths and description of cored intervals). The contact between the post-impact carbonates and impactites is marked by the horizontal line.

iron oxides and sulfides like magnetite, ilmenite, apatite, zircon, and sphene. Veins and cavity fillings and re-crystallized anhydrite clasts are present. Distinct types of melt clasts that indicate different basement granitic and gneiss protoliths are reported, some of which have planar deformation features. Major oxide chemical data for these impact melt rocks indicate medium- to- high-K calc-alkaline andesites to dacites (Figure 8).

4.2 Lithostratigraphic columns and logs

We revisited the lithostratigraphic columns, referring to the geophysical logs and petrographic and chemical analyses on core samples (Figures 8, 9).

In the Chicxulub-1 revised lithostratigraphic column, the sections from 505 to 805 m and 805 to 910 m are assigned to the Eocene and Paleocene, respectively. The section from 910 to 1080 m of marlstones and shales is in the Lower Paleocene. The sections from 1080 to 1275 m and 1275 to 1581.5 m are part of the impactite section, with the deep melt-rich unit (Figure 4).

The Sacapuc-1 SP log is characterized by high-frequency fluctuations superimposed on a low-frequency trend in the upper section of the post-impact carbonates (Figure 5). The post-impact sediments are formed by interbedded limestones and marlstones, and the contact with the impactite units lies at ~1000 m. The section below 1000 to 1527 m is characterized by low-frequency fluctuations. The upper part between 1000 and 1200 m is characterized by a broad minimum and is formed by sorted suevites. Marlstone layers are intercalated into the sequence at approximately 1040–1080 m and 1300–1320 m. At approximately 1420 m, a marked change in the SP log designates the contact with the melt-rich unit.

In the Yucatan-6 borehole, units forming the Paleogene post-impact carbonates, breccias and melt-rich breccias, and melt rocks marked in the self-potential logs (Figure 6) are characterized by high-frequency fluctuations superimposed on a low-frequency trend in the upper section of the post-impact carbonates. The section between 100 and 300 m is characterized by marlstones interbedded with calcarenites and calcirudists. This is followed by a thick limestone sequence. Between approximately 850 and 900 m, there are layers of calcarenites and calcirudists. The base of the

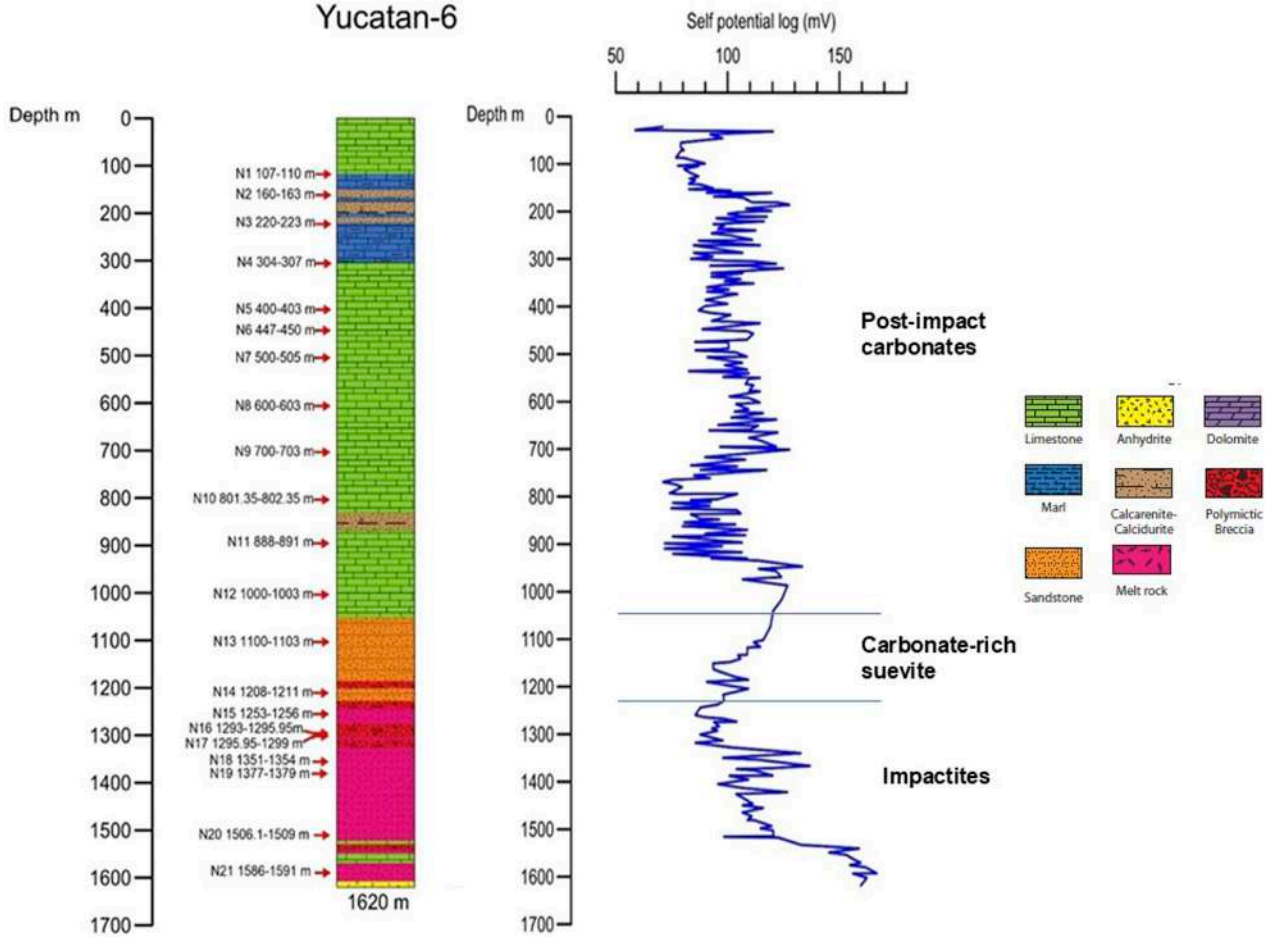

FIGURE 6
Lithological column and self-potential log for the Yucatan-6 borehole (see Figure 2A for the location of the drilling site and Supplementary Appendix A4 for information on depths and description of cored intervals). The contact between the post-impact carbonates and impactites is marked by the horizontal line.

sedimentary sequence is marked by the sandy unit described in the PEMEX report between 1080 and 1220 m, which shows distinct waveforms and frequency content (Figure 6). This is consistent with a breccia section, with varying characteristics with depth, carbonate contents, basement and melt clasts, apparent stratification and chemical composition, and textures as described above for the suevites (Claeys et al., 2003; Marín et al. (2001)). In the SP log, the top of the unit might extend upward to 1040–1000 m, as indicated by the trend, with a marked change above and below, with the bottom section from 1040–1080 m to 1220 m characterized by low-frequency fluctuations. If the low-fluctuating trend in the SP log corresponds to the sandy unit of sorted suevites, then that unit could extend upward to approximately 1000 m. It seems that the boundary between the sandy unit and the limestones in this lithostratigraphic column (Figure 6) may have been drawn rather arbitrarily as the mid-point between N12 and N13 without consideration of the SP log. The upper carbonate-rich suevite extends downward separated into two sections by a 1220–1240 m depth sorted suevite layer. Sorted breccias are also intercalated at the base from 1250 to 1280 m, marking the contact with the melt rocks.

4.3 Self-potential logs

The SP logs of the three boreholes show two distinct patterns of frequency–amplitude contents, characterizing the post-impact carbonate sequence and impactite units (Figure 9). The carbonate section is characterized by high-frequency components superimposed on a low-frequency signal. The post-impact carbonates in the Chicxulub-1 and Sacapuc-1 boreholes are limestones and marlstones, respectively, whereas in the Yucatan-6 borehole, the sequence is mainly composed of limestones. The Yucatan-6 upper section shows layers of marlstones, calcarenites, and calcirudists interbedded in the limestone sequence. The upper unit of the impact breccia sequence is represented by the carbonate-rich suevites (sandy unit), drilled between 1040 (1080) and 1220 m. The carbonate-rich suevites were not recognized in the Chicxulub-1 and Sacapuc-1 boreholes.

The impactite units are characterized by lower-frequency components with similar waveforms in the three boreholes, characterized by two broad minima. The impactites in the Chicxulub-1 and Sacapuc-1 boreholes are formed by an upper

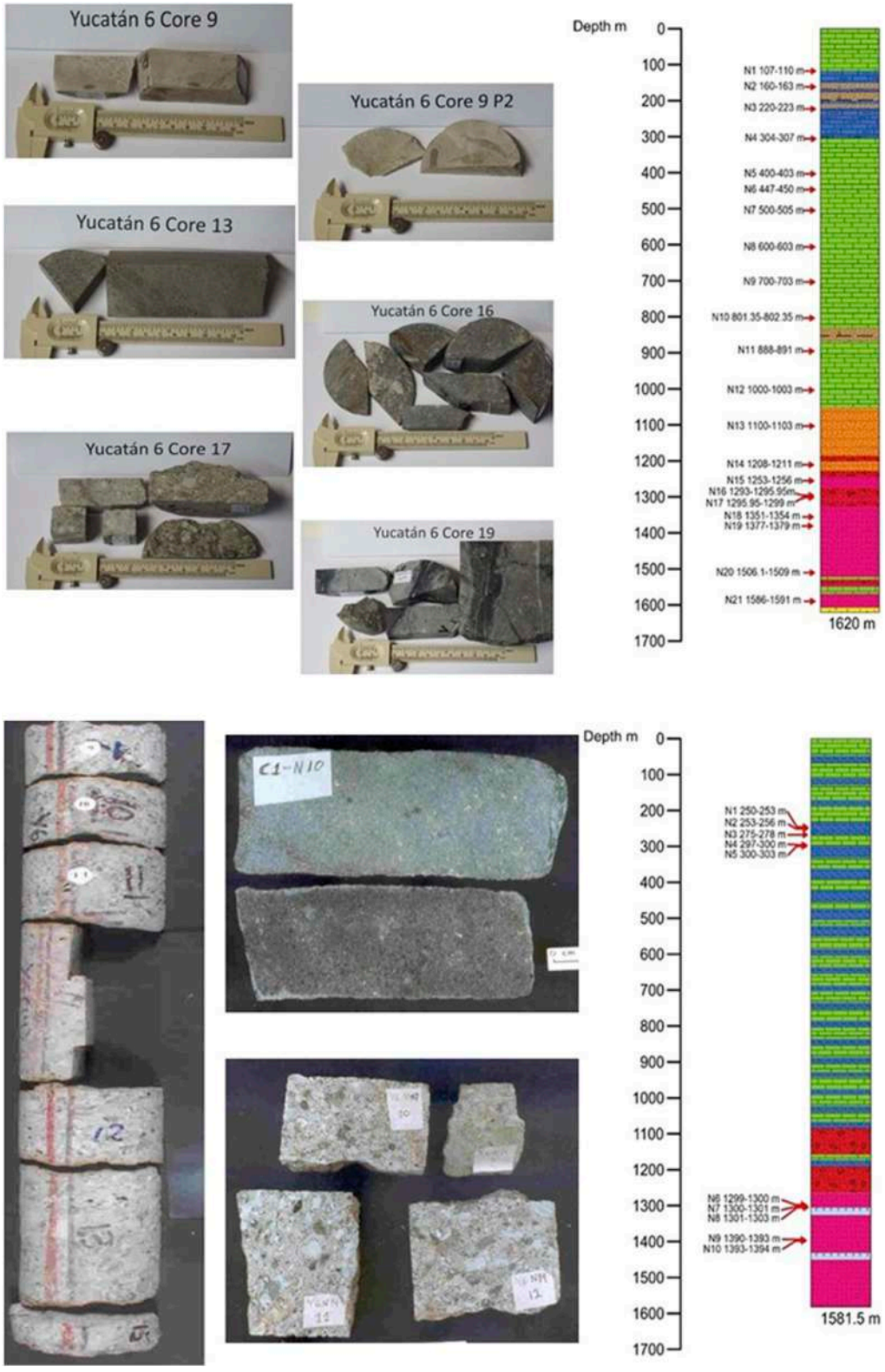

FIGURE 7
Core images for the Yucatan-6 borehole Y6–N14 interval and the Chicxulub-1 borehole C1–N10 interval.

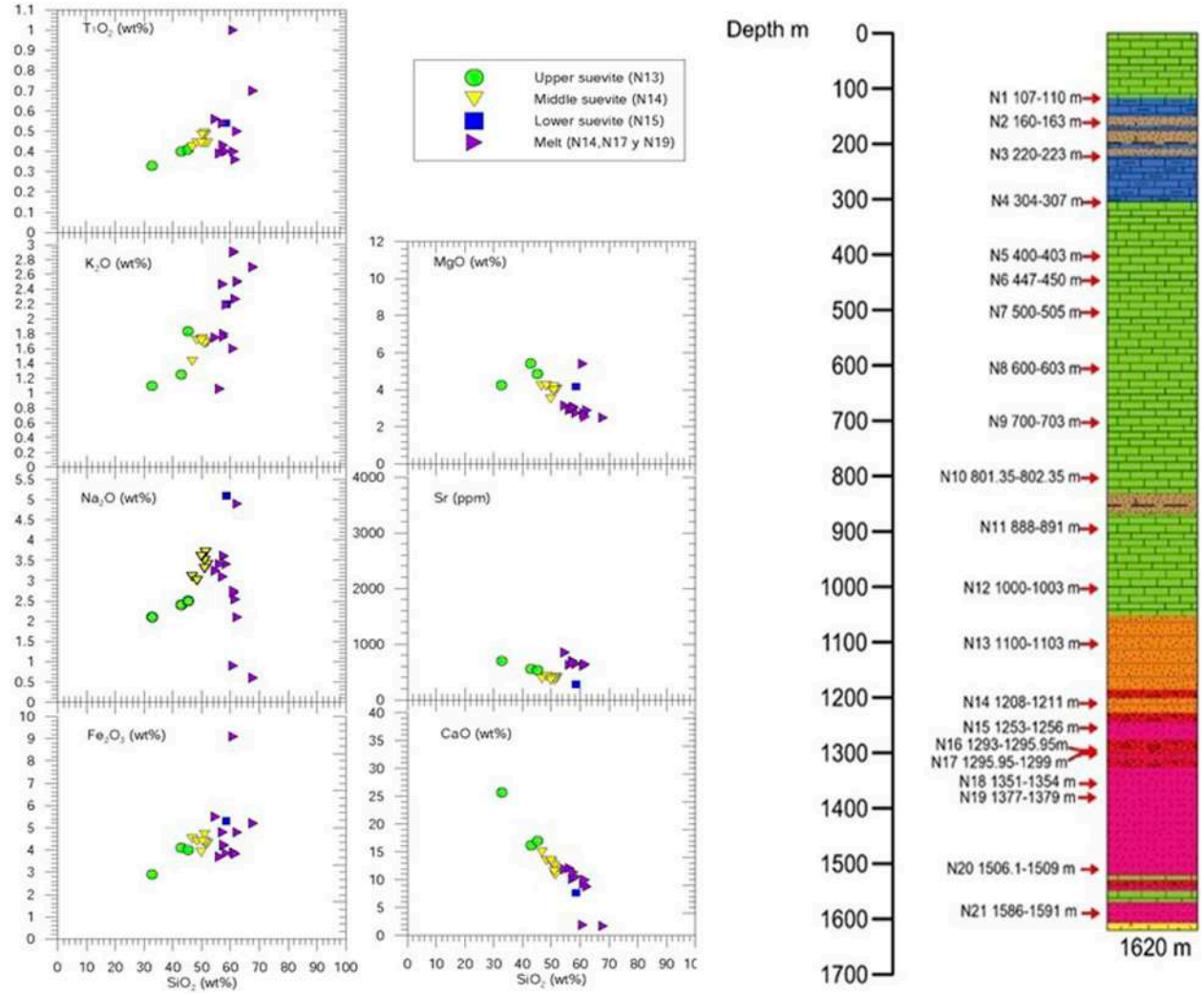

FIGURE 8
Major oxide chemical diagrams for samples of breccias and melt rocks from the Yucatan-6 borehole (Kettrup et al., 2000; Claeys et al., 2003). Data for the N13 Upper Suevite, N14 Middle Suevite, N15 Lower Suevite, and N14, N17, and N19 melt intervals. The Ca shows an inverse relation with Si contents. The sandy unit shows the highest Ca contents. The reference intervals are marked in the lithological column on the right. Depths and description of coring intervals are listed in Supplementary Appendix A4.

unit of sorted breccias and a lower melt and melt-rich unit, with intercalated marlstone layers. In the Yucatan-6 borehole, impactites are represented by melt and melt-rich breccias, with a limestone layer present toward the base of the melt rocks. The impactite–carbonate contact provides a reference marker for the lateral correlation.

The two broad minimums characterize the impactites and can be correlated in the logs of the three boreholes. The waveforms are better defined in the Chicxulub-1 and Sacapuc-1 boreholes. The relative maximum in-between the impactite section serves as a marker for the lateral correlation, located at 1190–1240 m in Chicxulub-1, at 1180–1230 m in Sacapuc-1, and at 1400–1435 m in Yucatan-6. In Yucatan-6, the log section below the Paleocene sequence from 1040 to 1620 m shows a more complex pattern, marking the presence of the sandy unit, and intercalated breccia layers in the melt and melt-rich units. The sandstone unit is distinguished by a linearly decreasing trend following the high-frequency fluctuations in the Paleogene carbonate sequence. The breccia units are marked by discrete relative maxima, whereas the thin limestone layers at approximately 1560 and 1600 m are marked by discrete relative minima.

Lateral correlations of Chicxulub-1, Sacapuc-1, and Yucatan-6 lithological columns and SP logs constrain the stratigraphy across the central zone, with the carbonate sections and impactites (Figure 9). The carbonate and impactite units can be traced across the annular trough. Lithological variations are more notable below 900 m, where the report describes a 400-m sequence of breccias in Yucatan-6 (?) compared to the 200-m sequence documented in Chicxulub-1. In Yucatan-6, the top of the melt unit was cut at 1260 m, whereas in Chicxulub-1, it was cut at 1275 m. The Sacapuc-1 SP log may indicate the possible presence of a sandy unit in this drill core at a depth of ~950 to 1000 m, characterized by low-frequency fluctuations (Figure 6).

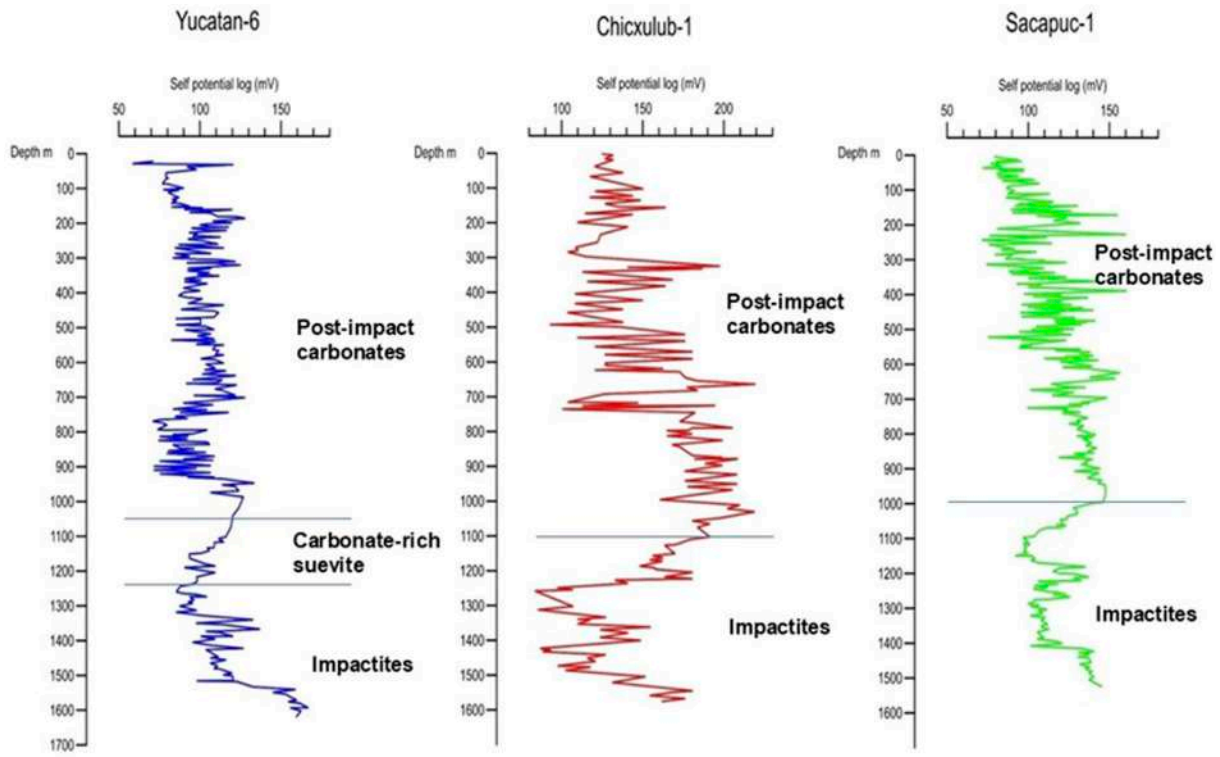

FIGURE 9
Self-potential (SP) logs for the Chicxulub-1, Sacapuc-1, and Yucatan-6 boreholes in the central sector. The proposed post-impact carbonate–impactite contact is indicated by the horizontal lines in the SP logs.

Further analysis of the SP logs uses spectral and wavelet transforms (Kumar and Foufoula-Georgiou, 1997; Pan et al., 2008), with changes in petrophysical properties determined from the distinct log responses. The logs show non-stationary behavior, and wavelet analyses on the log sections for the post-impact carbonates and for the impactites provide depth estimates for petrophysical property scaling (Figure 10).

4.4 Carbonate-rich suevites

The carbonate-rich suevites, initially described as green-gray sandstones with late Cretaceous foraminifera (López Ramos, 1983; Ward et al., 1995; Supplementary Appendix A4), lie at the bottom of limestone, bentonitic breccias, and the sandy unit, extending between 1000 and 1259 m in the Chicxulub-1, Sacapuc-1, and Yucatan-6 boreholes.

The carbonate clasts are of different types, angular to subangular, with dominant rounded dark micrites resembling intraclasts, mud pebbles, and aggregated grains. Fossil remains include Cretaceous foraminifera, algae, bivalves, gastropods, and sponges. Clasts composed of clay minerals and anhydrite are rare, as are basement fragments. The middle clast-rich suevite has larger contents and clast sizes, with a larger proportion of basement fragments. Clasts are unevenly distributed and composed of altered gneisses, schists, and quartzites, as well as quartz, melt particles, carbonates, anhydrite, and clay minerals. The unit displays several interesting features, including micrite clasts similar to those in the upper suevite and dolomite clasts. Claeys et al. (2003) noted the similarities between dolomite clasts in the Barton Creek Dolomite and those incorporated in the diamictite in Belize (Pope et al., 2005). Other features include dark brownish clasts with fluidal textures resembling rhyolite fragments, as interpreted by López Ramos (1983), presumably derived from rhyolite flows within the Yucatan basement, which might more likely represent altered impact melt fragments. Melt fragments with clay minerals represent 20% of the clasts and display variable degrees of alteration.

The unit is formed by clasts, with the matrix constituting approximately 30% and composed of fine-grained angular to sub-angular calcites, K-feldspars, plagioclases, and quartz. The lower suevite shows a distinct abundance of approximately 15% of shocked, altered basement clasts, silicate melt particles, and anhydrite in a fine-grained matrix of alkali feldspar, plagioclases, pyroxene, and quartz. Clasts are composed of quartz and feldspars, which display shock deformation features, including planar deformation features (PDF) and mosaicism. Gneiss and quartzite relics can be distinguished, with many partly digested in the matrix. Clinopyroxene rims on quartz and feldspars, described in Kring and Boynton (1992) in Y6–N17 melt fragments, are also present. Melt fragments show fluidal textures and occur in an isolated state or form aggregates, constituting 15% to 30% in thin sections.

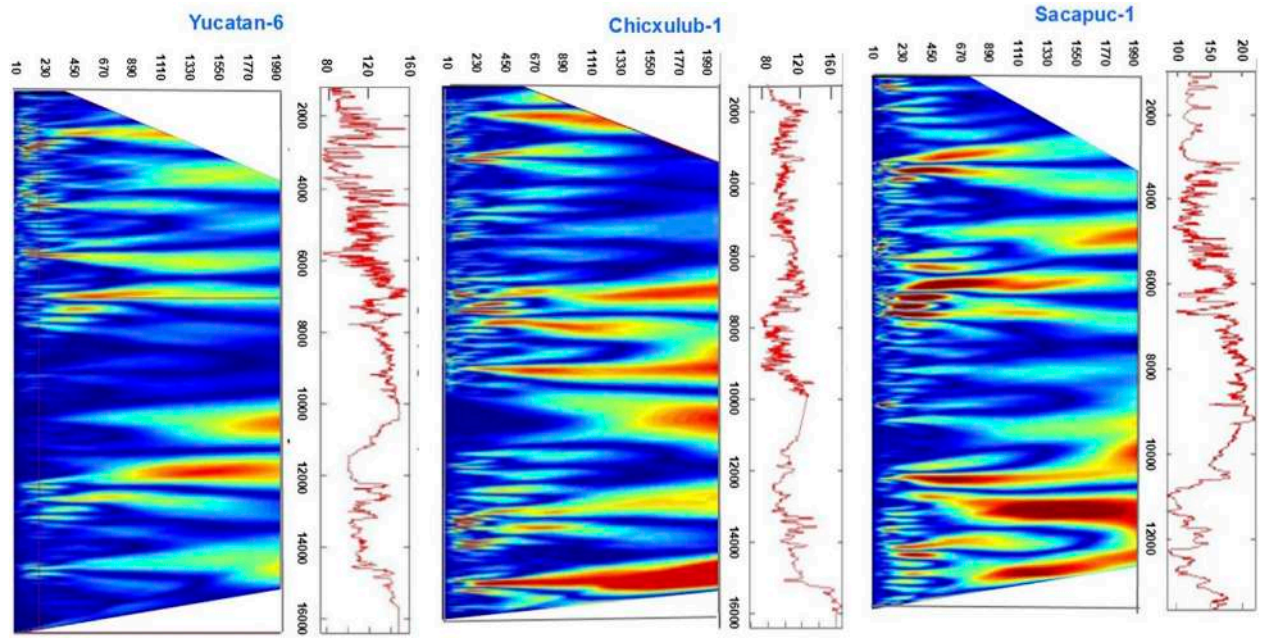

FIGURE 10
Wavelet transforms for the self-potential logs for the Chicxulub-1, Sacapuc-1, and Yucatan-6 boreholes in the central sector. Wavelet vertical axis, period in meters. Horizontal axis, SP log depth in meters.

4.5 Correlation with seismic data

Seismic reflection surveys have been conducted in the marine sector (Figure 11). The revised borehole columns and logs are correlated to the seismic reflection data. The seismic profiles are on the marine sector and boreholes are rotated assuming radial symmetry. The analyses of seismic stratigraphy have identified seismic packages which are correlated to the borehole columns. This has been used for the post-impact carbonates, identifying seismic stratigraphic units (Bell et al., 2004; Gulick et al., 2013; Whalen et al., 2014). For the study, the borehole data are correlated to the seismic images and seismic attributes. Analysis provides information on petrophysical properties for the impactite deposits and target lithologies.

Complex trace analyses, with instantaneous frequency, envelope amplitude, anelastic attenuation, and similarity attributes, are performed for the A and A1 lines (Salguero-Hernández et al., 2010; Salguero-Hernández et al., 2020). Seismic attributes enhance given features in seismic reflection data (Taner et al., 1979; Chopra and Marfurt, 2005). The instantaneous frequency attribute represents the average frequency of the amplitude spectrum of seismic traces, providing an estimate of impedance contrast and chaotic (un-coherent) reflections. High frequencies are associated to sharp impedance contrasts, with lower values for thin beds. The instantaneous frequency represents the time derivative of the instantaneous phase. The cosine of phase, represented by phase −1 to 1 signal along the seismic trace, is applied to emphasize the lateral continuity of reflectors and structural features. The phase for peaks, valley, and zero crossings of the seismic trace is followed by marking changes in the wavefront. Phase information is independent of the trace amplitude, and although trace amplitudes are weak, it enhances reflector lateral continuity, sample sequence boundaries, and strata geometry. The anelastic attenuation of seismic waves through a medium is a fraction of the energy lost per cycle (Dasgupta and Clark, 1998). The attenuation depends on the frequency, although it is weakly frequency-dependent in the range for short wavelengths. It relates to the physical properties of the propagating medium, providing information on the porosity, permeability, fluid saturation, pore pressure, and degree of fracturing (Dasgupta and Clark, 1998; Ramirez-Cruz et al., 2005).

5 Discussion

The early studies on Chicxulub were based on the drilling, logs, cores, and geophysical data from the PEMEX exploration program, which provided data and samples on the impact breccias and melt and on the stratigraphy and structure (Hildebrand et al., 1991; Hildebrand et al., 1998). The drilling reports were not openly available, and access to the drilling, logs, and cores was limited. This revision allows integrating early and recent studies on the Chicxulub structure and stratigraphy. Lateral correlations of lithological columns and geophysical logs are further constrained using geophysical models, seismic images, and attribute analyses.

Questions being addressed relate to the stratigraphy of carbonate and impactite sequences, their extent, distribution and thickness, and lateral continuity/discontinuity across the annular trough, particularly for melt pockets and sheet, and melt-rich and carbonate-rich breccia units.

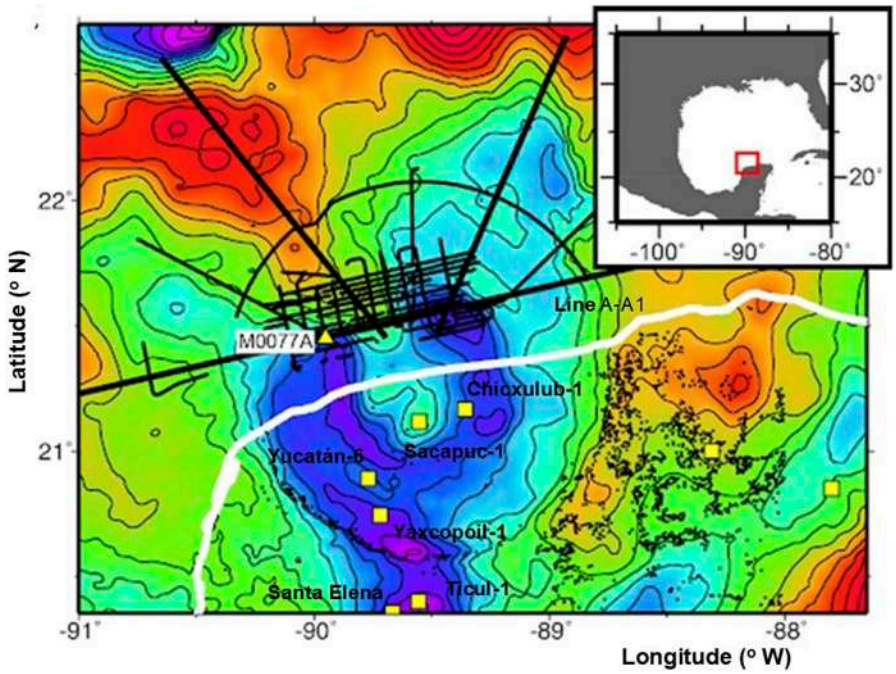

FIGURE 11
Chicxulub seismic experiments over the marine sector in the Yucatan platform (Morgan et al., 1997; Morgan et al., 2005; Gulick et al., 2008; Gulick et al., 2013). Seismic lines and 3D grid plotted on the gravity anomaly map (Morgan et al., 2017). Location of Chicxulub-1, Sacapuc-1, Yucatan-6, Yaxcopoil-1, Ticul-1, Santa Elena, and M0077A drilling sites and the regional seismic A-A1 line are marked.

5.1 Self-potential logs

Wavelet analyses of the SP logs provide constraints on the borehole lateral correlation (Figure 10). Spectral analyses of SP logs constrain the frequency contents of the signals. The units show characteristic frequency bands and trends that allow a lateral correlation between the boreholes across the central zone, peak ring, and annular trough. The SP log wavelets correlate with the lithological variations down column, constraining the frequency contents as a function of depth. The correlation of SP log waveforms is constrained from the frequency contents, using depth and physical property scaling information. The carbonates and impactites show distinct spectral signals, with layered carbonates showing characteristic frequency contents that separate them from the impactite response. The wavelet transforms for the upper and lower sections in Chicxulub-1, Sacapuc-1, and Yucatan-6 show the spectral responses of carbonates dominated by high frequencies in comparison to the impactites.

The extent, thickness, and characteristics of melt-rich units and the coherent melt sheet have been difficult to constrain from modeling of the potential field anomalies and in the seismic images. Kring (1995) estimated the thickness of the melt sheet and breccia units between ~3 and 7 km across the central zone and ~100 km in diameter within the transient cavity limits. Barton et al. (2010) reported modeling of the seismic reflection data imaging of the melt sheet in the central zone. The melt and melt-rich breccias appear limited to central magnetic anomalies (Pilkington and Hildebrand, 2000; Ortiz-Aleman and Urrutia-Fucugauchi, 2010). The borehole lateral correlation of melt-rich breccias and melt supports that units extend in the central zone across the peak ring into the Yucatan-6 borehole site (Figure 9). Seismic profiles record low seismic velocities and densities across the peak ring, which could represent rocks that have undergone fractures and hydrothermal alterations (Christeson et al., 2018; Riller et al., 2018).

Petrographic analyses on cuttings and cores show that the top of melt rocks was identified at 1260 m in Chicxulub-1, at 1425 m in Sacapuc-1, and at 1350 m in Yucatan-6. The correlation of the SP logs suggests the top of the melt lies at 1320 m in the Chicxulub-1 borehole, at 1420 m in the Sacapuc-1 borehole, and at 1580 m in the Yucatan-6 borehole. Correlation use of the characteristic frequency and waveform features in the SP logs is marked by two distinct lows separated by a well-defined double peak, which lies at 1190–1240 m in Chicxulub-1, at 1180–1230 m in Sacapuc-1, and at 1380–1420 m in Yucatan-6 (Figure 9).

Depth estimates place the intercalated limestone and anhydrite layers mainly within the melt-rich breccias and melt (particularly in the Yucatan-6 borehole). The melt rocks likely represent melt pockets distributed across the central zone and extended over the peak ring. Furthermore, the high-amplitude magnetic anomalies in the central zone suggest that the melt-rich suevites and melt rocks extend to the Yucatan-6 borehole. The frequency contents of the aeromagnetic anomaly indicate the presence of shallow (indicated by the high-frequency anomalies) and deep (indicated by the low-frequency anomalies with the inverted large dipolar anomaly) sources (Pilkington and Hildebrand, 2000; Ortiz-Aleman and Urrutia-Fucugauchi, 2010; Urrutia-Fucugauchi et al., 2022). Then, the shallow sources might encompass the melt-rich breccias

and melt pockets as well as the coherent melt sheet. Barton et al. (2010) considered the melt units drilled in the PEMEX boreholes to represent melt pockets, with the melt sheet located at a depth greater than 3 km. Gulick et al. (2013) interpreted the top of the melt sheet in seismic profiles as lying at approximately 1.5–2 km, beneath the impactite breccias.

5.2 Impactites

The Chicxulub-1, Sacapuc-1, and Yucatan-6 boreholes sample different sectors in the central zone and the annular trough. Lithological and mineralogical studies document differences across the structure. The compositional trends defined in the Yucatan-6 impactite section are different from those in the Yaxcopoil-1 borehole (Claeys et al., 2003). Schmitt et al. (2004) note that the Yucatan-6 middle suevite and the green melt subunit show different Fe_2O_3 and Al_2O_3 contents and also different CaO/MgO ratios. The compositional differences could be the result of differential degrees of hydrothermal alterations in the Yucatan-6 and Yaxcopoil-1 boreholes (Claeys et al., 2003; Schmitt et al., 2004; Kring et al., 2004; Stöffler et al., 2004). In the Yaxcopoil-1 borehole, the 861–885 m subunit in the ~100-m-thick impactite section is formed by green melt rocks. Kring et al. (2004) showed that the subunit is brecciated and altered, composed of microcrystalline Ca-rich pyroxene, plagioclase, and alkali feldspar, with minor concentrations of apatite, magnetite, rutile, calcite, barite, and phyllosilicates. Pyroxene and plagioclase compositions and xenocrysts and xenolith relative contents are similar to those in the Yucatan-6 melt (Kring and Boynton, 1992). Schmitt et al. (2004) note that the Yaxcopoil-1 impactite section, except for the green melt subunit, shows an increase in SiO_2, TiO_2, Al_2O_3, MgO, Fe_2O_3, Rb, Ni, Cr, and Zr contents and a decrease in CaO and Sr contents from the basal subunit to reworked subunit at the top.

The Yucatan-6 breccias are rich in melt and basement clasts, with different compositions and textures. Claeys et al. (2003) studied samples from core intervals Y6–N13, Y6–N14, and Y6–N15, documenting a stratification marked by varying composition, grain sizes, melt contents, and shocked lithic and mineral clast distribution. They distinguish an (a) upper unit described as a carbonate-rich suevite, with dominant, densely packed carbonate clasts and less basement fragments in a ~10 μm fine-grained matrix with calcite, plagioclase, quartz, K-feldspar, and amphibole; (b) a middle clast-rich suevite, with basement clasts and altered melt fragments with a trend to increase with depth in a more compacted, less porous matrix; (c) a lower thermo-metamorphic suevite formed by basement and evaporite clasts and abundant melt fragments in a recrystallized matrix of euhedral feldspar and pyroxene.

Major oxide and trace element analyses provide additional data, in addition to the drilling reports documenting andesitic to dacitic compositions (Figure 8). Schuraytz et al. (1994) reported petrographic and geochemical analyses for two core intervals in Yucatan-6 and one core interval in Chicxulub-1. The Y6–N17 and Y6–N19 samples described as melt-rich breccias show two textural distinct melt clasts within a matrix of subhedral-to-euhedral pyroxene and plagioclase micro-phenocrysts. The melt clast groups show matrix-like compositions or granitic-to-granodioritic gneiss protoliths. The C1–N10 sample is characterized by pyroxene and plagioclase phenocrysts in a coarse-grained matrix with no recognizable unmelted clasts. The samples from the C1–N10, Y6–N17, and Y6–N19 core intervals show distinct chemical compositions and textures, with differences in the matrix granulometry and porosity and in size and abundance of undigested clasts. The differences also include distinct contents of Ta, Co, Zr, Hf, and Sr and in the rare earth elements.

The SiO_2 content ranges from 54.8% to 61.7% in subsamples from the Y6–N17 and Y6–N19 intervals. SiO_2 is approximately 64.4% for a C1–N10 subsample. Schuraytz et al. (1994) also concluded that the presence of albite, quartz, K-feldspar, chlorite, epidote, and other phyllosilicates is indicative of hydrothermal alterations affecting the melt samples. Results show compositional variability in the matrix, clasts, and bulk samples, probably associated with varying relative contents of phenocrysts, quartz microxenoliths, and melted and unmelted clasts. Varying degrees of hydrothermal alterations contribute to the bulk compositional variability (Kring et al., 2004; Escobar-Sanchez and Urrutia-Fucugauchi, 2010).

Analyses of iridium and platinum group elements have been used to characterize the impactites and bolide nature. Koeberl et al. (1994) reported higher variable iridium contents in the impactites. Schuraytz et al. (1996) reported finding nuggets of the iridium metal in samples of Chicxulub-1 and Yucatan-6 impact melt rocks. Gelinas et al. (2004) reported Re-Os isotope analyses on impact melt breccias and lithic clasts from the Yaxcopoil-1 cores. The Os/Os ratios range from 0.19 to 2.3, with no indication of significant bolide contribution. Mixing calculations suggest that any bolide fraction was approximately 0.1% by mass. Tagle et al. (2004) reported low PGE contents in samples from Yucatan-6 and Yaxcopoil-1 cores, concluding that the bolide fraction in the impactites was below 0.05%. Furthermore, Feignon et al. (2022) report HSE analyses of drill cores from M0077A. These authors conclude that there is little evidence for an impactor component in the melt rocks on Chicxulub's peak ring (~0.01–0.05% meteoritic component in only one sample). Therefore, though initial studies indicated anomalous iridium contents (Koeberl et al., 1994; Schuraytz et al., 1996), the analyses on samples from Chicxulub-1 and Yucatan-6 cores show concentrations below analytical detection limits, with Ir contents around continental crust averages. Results constrain the bolide fraction incorporated in the melt, supporting little mixing in the impactites (Gelinas et al., 2004; Tagle et al., 2004).

The Santa Elena, Tekax, and Peto boreholes drilled in the southern sector documented the occurrence of two breccia sequences with distinct compositions and inverted stratigraphy (Figure 2) (Urrutia-Fucugauchi et al., 1996). The Santa Elena borehole located 110 km to the south from Chicxulub Puerto cut a thick melt-rich section without reaching its base. The borehole sampled the Paleogene carbonates and impactite section (Urrutia-Fucugauchi and Pérez-Cruz, 2008). The Tekax borehole cut the impactite section formed by an upper unit rich in melt and basement fragments in a melt-rich or carbonate-rich matrix and a lower unit rich in carbonate clasts in a carbonate-rich matrix. The two breccia units show an inverted stratigraphy similar to that documented in the Ries crater with the suevites and Bunte breccias (Horz et al., 1983; Stöffler et al., 2013; Sturm et al., 2013; Rebolledo-Vieyra and Urrutia-Fucugauchi, 2006). The lower carbonate Bunte breccias are cut in the Tekax and the Peto boreholes, which are located at

approximately 127 km and 152 km, respectively, from the center. The thickness of Bunte breccias cut in the Tekax and Peto boreholes is 354 m and 418 m, respectively. Models for breccia emplacement involve collapse of the central ejecta plume and lateral ejecta curtains (Wittmann et al., 2007). The ejecta plume contains a mixture of carbonate and silicate target rocks, whereas the ejecta curtains might form by carbonate-rich material (Wittmann et al., 2007; Urrutia-Fucugauchi et al., 2014).

The impact ejecta blankets on the Moon, Mars, or Mercury can extend long distances (Melosh, 1989). Ejecta blankets present significant differences for volatile-rich and volatile-poor targets, which show layered blankets characterized by longer runout deposits and lobe-like ramparts such as in Martian craters (Boyce and Mouginis-Mark, 2006; Sturm et al., 2013). As for the Ries crater, Sturm et al. (2013) have shown that the thickness of Bunte breccias, which are the deposits of a continuous proximal ejecta blanket, vary with distance, decreasing to a few meters at approximately 1.23 crater radii (Rc) forming the depression moat, followed by a steady increase to more than 100 m up to 1.45–2.12 Rc. Away from this concentric rampart ridge, the thickness decreases up to maximum distances of some 3.36 Rc. In the Chicxulub crater, ejecta deposits are not accessible because of the post-impact carbonate cover, which limits the mapping of the ejecta blanket. Farther away, outcrops are present in Albion Island and Rio Hondo at approximately 3.65 crater radii and in southern Mexico up to 4.7–5.2 crater radii at Armenia and Guayal sites (Pope et al., 2005).

The suevites show distinct characteristics from the underlying melt-rich and melt rocks as initially studied in samples from the Y6–N17 interval by Kring and Boynton (1992), Sharpton et al. (1992), and Schuraytz et al. (1994). The apparent complexity, mineralogy, and heterogeneous textures and composition in the clasts and matrix reflect the different sources in the excavated target stratigraphy, fluctuating temperature/pressure conditions, emplacement modes, hydrothermalism, and post-impact alteration (Claeys et al., 2003; Escobar-Sanchez and Urrutia-Fucugauchi, 2010; Gulick et al., 2017; Morgan et al., 2017; Riller et al., 2018).

5.3 Post-impact carbonate deposits—impactite contact

Determining the precise age of the contact between the impactites and the carbonate deposits that filled the basin has been crucial to determine the age of the impact (Smit et al., 2004; Arz et al., 2004; Keller et al., 2004; Whalen et al., 2020). After analyzing planktic foraminifera from well cuttings taken in PEMEX wells Yucatán 1, 2, 4, 5A, and 6, Ward et al. (1995) interpreted that the impact breccia belonged to late Maastrichtian. They identified several Maastrichtian species such as *Abathomphalus mayaroensis, Globotruncanita conica, Rosita patelliformis, Pseudoguembelina palpebra, Racemiguembelina fructicosa,* and *Hedbergella monmouthensis* in the breccia matrix, concluding that its presence indicates a late Maastrichtian age for deposition of this unit. The most modern of these species is *A. mayaroensis*, whose first and last appearances were dated, respectively, in 69.18 Ma and 66.04 Ma (=K/Pg boundary) according to the time scale GTS2012 (Gradstein et al., 2012). So the presence of *A. mayaroensis* in the breccia matrix, as cited by Ward et al. (1995), only indicates a minimum (not univocal) age of the late Maastrichtian. However, given the hybrid and detrital nature of the impact breccia, these species must be considered reworked (*ex situ*) as a result of the erosion of older rocks (Arz et al., 2022). The absence of Danian planktic foraminiferal species is compatible with a K/Pg age for the impact breccia inside the Chicxulub structure (Kuiper et al., 2008).

Moreover, Ward et al. (1995) assumed that the impact breccias are overlain in the Chicxulub-1 borehole by a marly unit of ~18 m containing *in situ* late Maastrichtian planktic foraminiferal assemblages reported by López Ramos (1975) and López Ramos (1983). These assemblages are composed by *Globotruncana rosetta, Globotruncana ventricosa, Globotruncana lapparenti, Globotruncana fornicata, Pseudoguembelina excolata, Heterohelix globocarinata, Pseudotextularia elegans, Planoglobulina carseyae,* and *Globigerinelloides volutus*). It should be noted that the last appearances of *G. lapparenti* and *G. ventricosa* have been dated, respectively, in 70.90 Ma and 70.14 Ma, both ages older than the first appearance of *Abathomphalus mayaroensis* (69.18 Ma), recorded in Ward et al. (1995) in the matrix of the underlying impact breccia. These age inconsistencies can be explained by assuming that all the planktic foraminiferal specimens are reworked (*ex situ*) and cannot be used to date this unit (Arz et al., 2022).

Ward et al. (1995) only analyzed two breccia samples from Yucatan-6, but none from Chicxulub-1, Sacapuc-1, Yucatan-6, and Ticul-1. In the Yucatan-6 borehole, the impactites are overlain by a greenish gray sandy unit, which is not present in the Chicxulub-1 and Sacapuc-1 boreholes (Figure 7). This unit was described in the PEMEX drilling report as bentonitic carbonate sandstones with Upper Cretaceous microfossil assemblages. The unit includes cores Y6–N13 (1200–1203 m) and Y6–N14 (1208–1211 m), formed by sand-sized grains of carbonates and altered silicates cemented in a calcium carbonate matrix, is considered a carbonate-rich sorted suevite. The silicate clasts show evidence of planar deformation, observed in quartz, plagioclase, and zircons (Sharpton et al., 1992; Krogh et al., 1993).

Marín et al. (2001) examined samples from the intervals Y6–N12 (1000–1003 m), Y6–N13 (1200–1203 m), and Y6–N14 (1208–1211 m). After analyzing the planktic foraminiferal assemblages in thin sections, Marín et al. (2001) proposed that the interval Y6–N12 was of the Damian age. They indicated the presence of the following Danian species (expressed in updated generic nomenclature): *Globanomalina compressa, Parasubbotina pseudobulloides, Acarinina trinidadensis*? (or possibly *Acarinina uncinata*), and *Subbotina triloculinoides*. Although they only illustrated thin section microphotographs of probable specimens of *Parasubbotina pseudobulloides* and *Chiloguembelina* sp., the proposed age is compatible with the one determined with greater precision in Yaxcopoil-1 and M0077 boreholes for the equivalent stratigraphic interval (Arz et al., 2022). This interval represents normal post-impact sedimentation and early infill. Samples from the underlying intervals Y6–N13 and Y6–N14 show reworked assemblages of orbitoids (benthic macroforaminifers), mollusk, and algal fragments of a shallow water assemblage. The sandy unit in the PEMEX report extends between 1220 and 1080 m (Supplementary Appendix A4). Based on the SP log, the sandy unit extends upward to 1040 m. The SP log shows a conspicuous linear trend from low to high values toward the top, suggesting a

graded upward sequence (Figure 9). The reworked unit could be derived from the peak ring that lies in between the central zone and the annular gravity low. Formation of the peak ring elevated topography could provide depositional conditions for the sandy unit, which could explain why it is not present in other boreholes. We note that in the SP log of the Chicxulub-1 borehole, there is an interval of increasing values that corresponds to a sequence of marlstones and shales, which extends from approximately 1080 to 930 m (Supplementary Appendix A4). This was considered to correspond to the base of the Paleocene section at 930 m documented in the paleontological reports. The nature of the unit and stratigraphic implications are further discussed below in terms of the models of peak ring formation and extent of the melt and melt-rich units.

The depth to the top of the impact breccias in the Chicxulub-1 and Sacapuc-1 boreholes lies at 1100 m and 1000 m, respectively. The depth to the impact breccias in the Yucatan-6 borehole is deeper, at 1220–1250 m, suggesting a discontinuity (Figure 6). The difference in the stratigraphic series is the sandy unit in the Yucatan-6 at 1080 m (PEMEX reports) or at 1040 m (as suggested from the SP log). If the unit represents a carbonate-rich suevite (Claeys et al., 2003), then the top to the impact breccias lies at comparable depths across the peak ring within the central sector. The presence of Danian planktic foraminifera and absence of shock deformation oppose representing re-worked breccias (Marín et al., 2001). From the analysis of the SP log and lateral correlation indicated by similar low-frequency waveforms in the SP logs of the three boreholes (Figures 9, 10), we concur with the interpretation by Claeys et al. (2003) that the unit is carbonate-rich suevites. The unit formed by altered silica-rich sand-size clastic within a clastic matrix is not a Late Cretaceous sedimentary unit, as described in previous reports by Ward et al. (1995) (Supplementary Appendix A4). The unit is marked by a linear increasing trend in the Yucatan-1 SP log, not observed in the Chicxulub-1 and Sacapuc-1 logs. The lateral correlation of borehole logs provides marker horizons that permit assessing stratigraphic completeness within the impactites, post-impact carbonates, and impactite–carbonate contact. Logs also record the relative complexity in the breccias section, with the intercalated layers of carbonates and ash glassy layers. The lateral correlation of the impactite sections has implications for the peak ring models and post-impact modification processes during the collapse and post-impact stages, recorded in the central zone.

5.4 Seismic attributes

Instantaneous attributes were determined for the A and A1 lines across the basin (Figures 11, 12; Salguero-Hernández et al., 2010; Salguero-Hernández et al., 2020). The western line crosses the peak ring from the central sector into the annular trough. We extend the study, using the post-stack complex trace instantaneous phase, instantaneous frequency, envelop amplitude, and similarity attributes.

The instantaneous frequency and instantaneous phase (Salguero-Hernández et al., 2020) and the similarity and instantaneous envelop attributes for seismic line A are shown in Figure 12. The Yucatan-6 borehole has been rotated to its relative position along the seismic profile, assuming rotational symmetry of the structure, and the bathymetric high of the peak ring is used as a further constraint for the correlation. Joint analyses of marine seismic reflection data and onshore boreholes and logs have used this approximation (Bell et al., 2004). Whalen et al. (2014) in their analysis of the seismic and stratigraphic units in the seismic images and the Yaxcopoil-1 borehole analyzed an alternative correlation in the eastern sector. Here, we adopt a correlation in the western sector proposed by Bell et al. (2004).

Seismic attributes show a sharp contrast in response for the post-impact carbonate sediments that fill the basin and the underlying units. The instantaneous frequency attribute enhances physical property variations for the deep material in the central sector and the western sector. In the instantaneous-phase attribute, infill carbonate sediments are characterized by reflectors with distinct lateral continuity and variable thickness. Stratigraphic packages are distinguished in the instantaneous frequency attributes, with lateral changes across the profile. The similarity attribute shows the coherence and dissimilarity in adjacent seismic reflectors, measuring lateral continuity, useful to identify fractures and faults. The contact between the breccias and the overlying carbonates is marked in the seismic attribute responses, suggesting a thin transitional layer with high-energy reflectors delineating a surface relief over which the sediments were deposited.

The post-impact sediments show weak impedance contrasts and attenuation at most frequencies. High frequencies and attenuation factors mark the sediment packages following the high-energy reflectors that follow the basin floor characterizing the basin sediment fill. The intermediate and basal sediments show high impedance contrast and low frequencies, which mark the contact with the basin floor at depths from 800 to 1100 m. The melt- and basement-rich breccias in the central sector and the terrace zone show high-amplitude impedance contrasts and low frequencies. The peak ring is characterized by high frequencies (between 20 and 30 Hz) and high attenuation factors (between 0.6 and 1). Deeper units show intermediate to high frequencies and high attenuation factors.

5.5 Yucatan basement

The lack of surface exposures has hampered studies on the basement of the Yucatan Block, which has been investigated by conducting deep drilling and geophysical surveys. Paleozoic rocks and granites are exposed in the southeastern part of the Yucatan Block, mainly in the Maya Mountain in Belize. According to the data on the age of detrital zircons and the Nd isotopes, high-grade metamorphic outcrops in Chiapas and Guatemala are mainly of Grenvillian affinity. The basement has Pan-African affinity and is correlated to the Sewanee terrane in Florida. Tectonic reconstructions place the Yucatan Block close to the Ouachita Orogenic Belt during the pre-rift opening of the Gulf of Mexico in the Middle Jurassic (Zhao et al., 2020). The counter-clockwise rotation of the Yucatan block during the opening of the Gulf of Mexico displaced the block to a southern position (Pindell and Dewey, 1982; Molina-Garza et al., 1992).

The zircon ages from Chicxulub drill cores and from K/Pg boundary sections cluster at 545–550 Ma, recording a

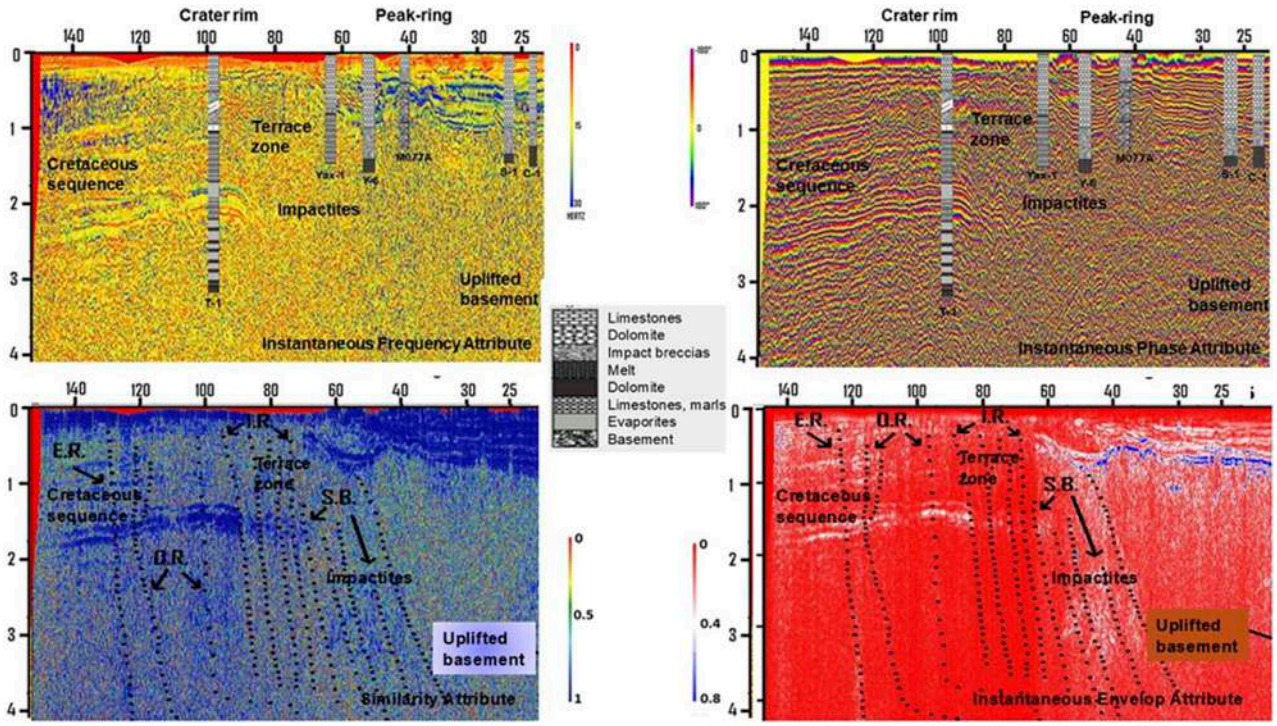

FIGURE 12
Seismic sections with complex trace attributes across east–west line A-A1 (Morgan et al., 1997; Salguero-Hernández et al., 2020). Instantaneous frequency, instantaneous phase, instantaneous envelop, and similarity attributes for the Chicxulub seismic line A over the Chicxulub western sector (Salguero-Hernández et al., 2020 and this work). ER, exterior ring; OR, outer ring; IR, inner ring faults; SB, slump blocks. The position of the Yaxcopoil-1 (Yax-1), Chicxulub (C1), Sacapuc-1 (S1), Yucatan-6 (Y6), and Ticul-1 (T1) boreholes in rotated coordinates assuming radial symmetry of the structure. The line crosses the peak-ring, terrace, and rim zones.

crystallization age (Kamo et al., 2011). The basement is lithologically heterogeneous, as indicated by basement clasts recovered in Chicxulub suevites with granites, dolerites, gneisses, quarzites, amphibolites, and quartz–mica schists (Kettrup et al., 2000; Keppie et al., 2011; Urrutia-Fucugauchi et al., 2011; Schmieder et al., 2018; Zhao et al., 2020). Melt rocks present wide ranges in chemical composition and strontium and neodymium isotopes, supporting a heterogeneous target (Kettrup et al., 2000). Boreholes drilled in the central zone sampled impactite units, sampled at depths of approximately 900–1000 m extending downward to the maximum drilled depths of 1581 m in Chicxulub-1, 1527 m in Sacapuc-1, and 1645 m in Yucatan-6. The Yaxcopoil-1 borehole in the southern terrace zone drilled a ~100-m-thick impactite section overlying Cretaceous target sediments, likely representing displaced carbonate blocks of the mega-breccia sequence between 900 m and 1511 m (Urrutia-Fucugauchi et al., 2004). The M0077A borehole reached a depth of 1334 mbsf (meters below seafloor), recovering basement, melt rocks, suevites (breccia with melt fragments), and post–impact sediments (Morgan et al., 2016). The drill section was divided into three main stratigraphic units from top to bottom: (1) Cenozoic sediments (505.7–617.33 mbsf); (2) suevites and impact melt rocks (617.33–747.02 mbsf); (3) granitoids (747.02–1334.69 mbsf) intruded by felsic and mafic dykes such as felsite and dolerite (Zhao et al., 2020). The thickness of impactite is more than 700 m.

Basement rocks were reached in the Yucatan-1 and Yucatan-2 boreholes in the central Yucatan peninsula and the Yucatan-4 borehole in the eastern sector (Figure 2). Metamorphic crystalline rocks were drilled at the bottom of the boreholes, at approximately −3226 m in Yucatan-1, −3488 m in Yucatan-2, and ~2400–2426 m in Yucatan-4.

The impact excavated a deep transient cavity, with fragmented material ejected from different target depths. The breccias show melt-rich or carbonate-rich matrices. Basement clasts are not only mainly granitic but also include granodiorites, diorites, gneiss, amphibolite, quartzites, and schists with distinct degrees of alteration. Clasts in the breccias provide a sampling of the basement from distinct levels, which have been investigated in mineralogical and geochemical studies. Kettrup et al. (2000) analyzed melt rocks from Chicxulub-1 and Yucatan-6, which show variable contents in Al, Ca, and alkalis, with the SiO_2 content ranging from 58 to 63 wt%. The basement clasts in Yucatan-6 come from Y6–N14 and Y6–N16. The Y6–N14 is a high-plagioclase clast with an SiO_2 content of 69 wt% and $Na_2O + K_2O$ of 9.2 wt%, and the "annealed and recrystallized fragment" from Y6–N16 has an SiO_2 content of 62 wt% and $Na_2O + K_2O$ of 7.3 wt%. The Nd isotopic ratios for melt and basement clasts group within a narrow range of 0.5123 to 0.5124 (Kettrup et al., 2000). Kettrup et al. (2000) proposed that the high CaO_2 contents can be accounted for by the contribution of target carbonates, whereas intermediate-to-mafic

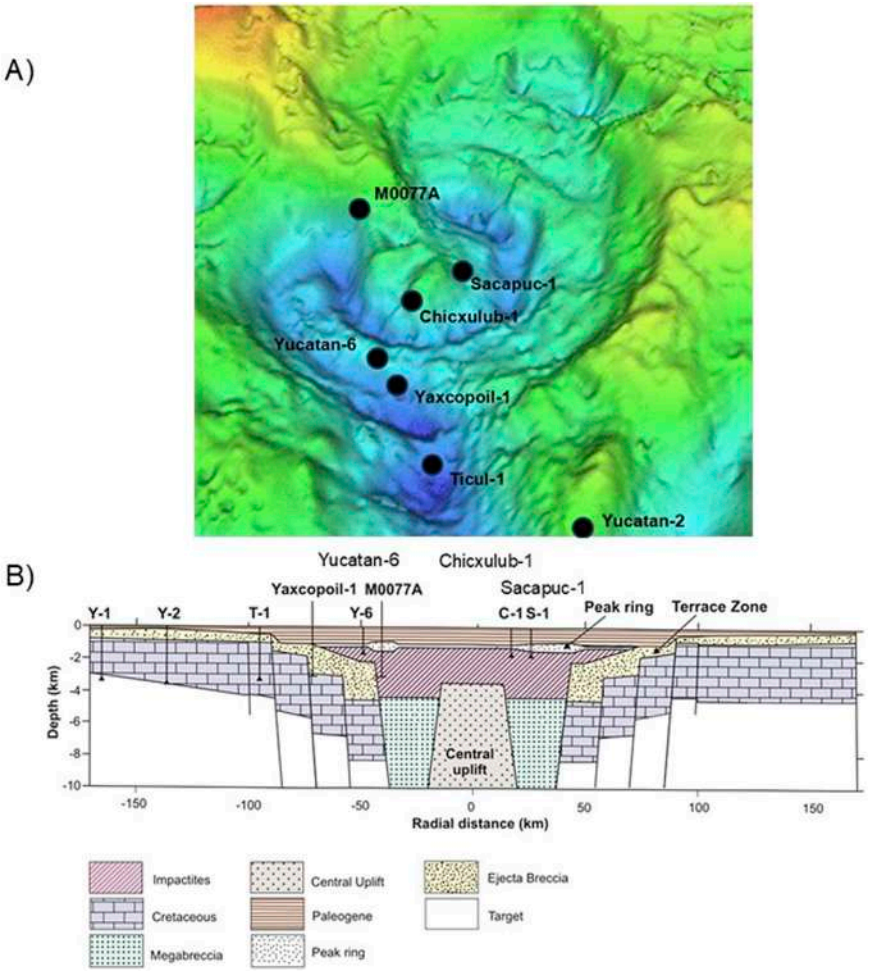

FIGURE 13
(A) Location of drilling sites for Chicxulub-1, Sacapuc-1, Yucatán-6, Yaxcopoil-1, M0077A, Ticul-1, and Yucatan-2 boreholes, plotted on the gravity anomaly (Sharpton et al., 1993). Chicxulub-1 and Sacapuc-1 boreholes are located in the central zone, with the Yucatan-6 located across the annular trough. **(B)** Schematic cross-section, showing the structure of the post-impact basin, central uplift, peak ring, terrace zone, fault zone, impact breccias, and melt (modified from Hildebrand et al., 1998; Urrutia-Fucugauchi et al., 2025). The target section is formed by carbonate sediments and granitic basement rocks. The characteristics and distribution of melt sheet and breccias are constrained from geophysical models and boreholes (see recent models in Christeson et al., 2021) The structure and stratigraphy of the peak ring is constrained from the M0077A borehole (Morgan et al., 2016; Morgan et al., 2017).

lithologic rocks are needed to account for the relatively high Fe and Mg contents in the melt clasts. The geochemistry and mineralogy of the suevites, including the melt and lithics examined in the Yaxcopoil-1 borehole, provide additional constraints on chemical variations (Kring et al., 2004; Tuchscherer et al., 2004).

Keppie et al. (2011) analyzed zircons from granitic and graniodiorite clasts from the Yaxcopoil-1 borehole. U-Pb dates vary from 546 + 5 Ma to 465 Ma, with three discordant younger ages between 345 and 130 Ma. The 546 Ma date is interpreted as an intrusion age, which is consistent with U-Pb dates on zircons obtained by Krogh et al. (1993), Kamo and Krogh (1995), and Kamo et al. (2011). For the peak ring basement section, Zhao et al. (2020) report U-Pb dates on zircons from a granite sample at 1200 m depth, with a mean age of 340–8 + 9.9 Ma from a concoidal diagram for 24 zircon dates. Zhao et al. (2020) calculated a mean zircon age of 326 ± 5 Ma from 40 concordant zircon grain ages through the whole section. These ages contrast with the 500–545 Ma obtained from zircons from the other boreholes (Kamo et al., 2011). Zhao et al. (2020) proposed that the granites originated from the bottom of the excavation cavity and represented little in the ejecta, collapsing outward to the site of the peak ring. The numerical model from Morgan et al. (2016) was analyzed by Riller et al. (2018) and Rae et al. (2019), and it was indicated that granites come from the transient cavity wall, with a vertical depth of ~8–10 km and horizontal distances of ~20 km relative to the impact site, moving outward to the wall of the transient cavity and then collapsing inward to form the peak ring. If granites came from the displaced zone during formation, it explains why there were few zircons with ages of approximately 340 Ma. Keppie et al. (2011) suggested for their three discordant younger ages, 340 to 130 Ma obtained from a granitic clast from the Yaxcopoil-1 breccias that ages reflect impact effects. Krogh et al. (1993) also reported an age of 320 Ma for a zircon grain, suggesting it was affected by shock effects. Shock microstructures on zircons from the Chicxulub peak ring

basement section have been analyzed, with studies constraining the melt dynamics and resurge-induced effects and porosity and microfracturing (Wittmann et al., 2021; Timms et al., 2019), and further work will help in evaluating the chronological data. The 550 to 545 Ma igneous rocks have not been reported for the Maya Mountains in Belize and the terranes in southern Mexico. Their tectonic association has been discussed, related to an Ediacaran arc in northern peri-Gondwana (Keppie et al., 2011).

5.6 Central structure

The deep crustal structure investigated using gravity, magnetics, and seismic reflection data shows the impact-induced deformation processes (Hildebrand et al., 1998; Christeson et al., 2001; Batista et al., 2013; Gulick et al., 2013). Large impacts produced a transient excavation cavity deep into the crust, with deformation, fragmentation, and ejection of the crustal material (Melosh, 1989; Melosh and Ivanov, 1999; Pierazzo and Melosh, 2000; Urrutia-Fucugauchi and Pérez-Cruz, 2009). The major structural element is the central uplift, 40–60 km in cross-sectional diameter and 9–20 km in vertical uplift. The uplifted lower crust is characterized by a strong gravity anomaly and an inverted magnetic dipolar anomaly, which have been modeled with contrasting results (Sharpton et al., 1993; Pilkington et al., 1994; Hildebrand et al., 1998; Vermeesch and Morgan, 2008; Ortiz-Aleman and Urrutia-Fucugauchi, 2010; Gulick et al., 2013). Seismic reflection profiles show that the Moho is uplifted by approximately 1 km, associated with the excavation of the transient cavity and its collapse, with crustal faults extending into the lower crust associated with the terrace zone, and down-faulted slump blocks (Christeson et al., 2001).

Inward dipping reflectors cut the zone beneath the peak ring into slump blocks. The peak ring shows distinct lithologies marked in the seismic velocities with a top low-velocity layer 0.6–0.8 km/s lower than in the carbonate sediments and high-velocity zones in the adjacent annular trough with an abrupt decrease in the velocity in the dipping reflector zone. Beneath a depth of ~0.5–2.5 km, velocities are lower than those toward the central basin units, which correlate with the annular gravity low, indicating lower densities and possibly fractured rocks. The models proposed for peak ring formation involve the interaction of two deformational regimes with the inwardly collapsing transient cavity rim and outwardly collapsing central uplift. The peak ring is formed by overturned fractured and brecciated basement rocks (Collins et al., 2008; Collins et al., 2020; Urrutia-Fucugauchi and Pérez-Cruz, 2009; Morgan et al., 2016; Morgan et al., 2017; Gulick et al., 2013).

In the seismic 3D grid, the velocity model is characterized by an increase of velocity from 4.0 to 5.5 km/s beneath the peak ring (Morgan et al., 2016; Morgan et al., 2017). On the outward zone, inclined sets of reflectors dip beneath the peak ring toward the central zone. Beneath the peak ring top marked by the boundary deposits of basin floor, velocities are lower, delineating a broad zone inclined and extended toward the central zone. In the central zone beneath the impact breccias, a dipping high-energy reflector interpreted as the top of the melt lies at a depth of 1.2 to 1.7 km, correlating with the melt contacts in the Yucatan-6, Chicxulub-1, and Sacapuc-1 boreholes.

The schematic cross-section across the Chicxulub structure shows stratigraphic units and boreholes, with the upper 3-km section constrained from the regional correlation of lithological columns (Figure 13). The cross-section shows the asymmetries in the basin, fault zones, central uplift, and the structure and stratigraphy in the central zone.

Drilling programs have reached the post-impact carbonates, impact breccias, melt, and basement in different sectors and adjacent areas. The suevites and carbonate-rich Bunte breccias with the inverted stratigraphy were drilled outside the rim in the southern sector (Tekax and Peto boreholes). The target Cretaceous carbonates have been drilled in the megablock unit in the southern terrace zone (Yaxcopoil-1 borehole). The uplifted granitic basement and igneous and impact dykes were drilled in the peak ring. Drilling programs have provided useful constraints; however, further efforts are needed. Integrated analyses and inversion models of geophysical data and drilling will further constrain the stratigraphy and subsurface structure.

6 Conclusion

We review and analyze unpublished data, geophysical logs, and lateral correlations for boreholes Chicxulub-1 (1581.5 m), Sacapuc-1 (1527 m), and Yucatan-6 (1645 m) to characterize the central sector structure and stratigraphy. The structure and impactite units are not exposed at the surface, and drilling and coring have been critical in providing data and samples for characterization and laboratory analyses. The boreholes provided the initial evidence on the buried structure, and the cores were critical for the subsequent studies confirming the impact origin and age at the K/Pg boundary.

Inconsistencies in the biostratigraphy of Cretaceous planktic foraminiferal species previously reported in the breccia matrix in Yucatan 1, 2, 4, 5A, and 6 boreholes, and in the marly unit that overlies the impact breccias in Chicxulub-1, are evidence of reworking and cannot be used for dating the Chicxulub impact. The planktic foraminiferal assemblages reported in the interval Y6–N12 (1000–1003 m) of Yucatan-6 borehole underpin a Danian age for the first post-impact carbonates. We conclude that planktic foraminiferal biostratigraphic data reported in the central sector are compatible with a Cretaceous/Paleogene age for the Chicxulub impact.

The PEMEX boreholes remain the deepest drilled in the central sector. The self-potential logs characterize the carbonate and impactite sections, showing that units can be traced across the central zone. The Chicxulub-1 and Sacapuc-1 boreholes reached the impactite units at ~1100 m and ~1000 m, respectively. The Yucatan-6 borehole sampled the impactites from ~1040 to 1080 m considering the re-worked carbonate-rich suevite. The impactite sections in the central area have a thickness greater than 500 m. The PEMEX boreholes ended within the impactite section, without reaching the Cretaceous carbonates.

The borehole and log correlations constrain the stratigraphy, extent, and distribution of melt-rich breccias and melt across the central sector, confirming that melt rocks extend across the annular trough and peak ring. Analysis of the logs and cores shows that the transitional carbonate-rich unit in the Yucatan-6 borehole is a

carbonate-rich sorted suevite, which correlates with the carbonate-rich sorted suevite in the M0077A, across the annular trough. The revised columns, core data, and logs provide further insights on the stratigraphy of the post-impact carbonates and impact breccias and melt.

Data availability statement

The original contributions presented in the study are included in the article/Supplementary Material, further inquiries can be directed to the corresponding author.

Author contributions

JU-F: Conceptualization, Investigation, Methodology, Writing – original draft, Writing – review and editing, and Formal analysis. LP-C: Conceptualization, Formal analysis, Investigation, Methodology, Writing – original draft, and Writing – review and editing. AW: Formal analysis, Investigation, methodology, Writing – original draft, and Writing – review and editing. JA: Investigation, Methodology, Writing – original draft, and Writing – review and editing. IA: Investigation, Methodology, Writing – original draft, and Writing – review and editing. LX: Formal analysis, Investigation, Methodology, Writing – original draft, and Writing – review and editing. JZ: Formal analysis, Investigation, Methodology, Writing – original draft, and Writing – review and editing. VG: Investigation, Methodology, Writing – original draft, and Writing – review and editing. ES-H: Formal analysis, Investigation, Methodology, Writing – original draft, and Writing – review and editing.

Funding

The author(s) declare that financial support was received for the research and/or publication of this article. J. Arz and I. Arenillas acknowledge grants PID2022-136233NB-I00 by MCIN/AEI/10.13039/501100011033 and ERDF A way of making Europe, and DGA group E33_23R, Aragonese Government and ERDF A way of making Europe. Vicente Gilabert acknowledges support from Ministerio de Universidades (MIU) and European Union (Margarita Salas post-doctoral grant) funded by European Union Next-Generation EU. Thanks to the Government of Yucatan and IODP-ICDP Chicxulub Expedition 364 drilling project. We acknowledge support of the UNAM-COPO Chicxulub marine geophysics and oceanographic campaigns and the Chicxulub Science Foundation FCC-22–002. This is publication IICEAC-24–010.

Acknowledgments

The study is part of the Chicxulub and K/Pg Boundary Program and Chicxulub Institute for Advanced Studies (IICEAC) of Yucatan. We acknowledge useful review comments by Christian Koeberl, two reviewers and editor Andrea Zanchi. We acknowledge access to PEMEX drilling reports and data. We acknowledge contributions and useful discussions with Antonio Camargo-Zanoguera, G. Perez Drago, A. Gutierrez Silos, A. Reyes, I. Canales, E. Escobar, and Chicxulub UNAM student group. Assistance was provided by Miguel A. Diaz, Marysol Valdez, Rafael Venegas and A. Escalante.

Conflict of interest

The authors declare that the research was conducted in the absence of any commercial or financial relationships that could be construed as a potential conflict of interest.

The author(s) declared that they were an editorial board member of Frontiers, at the time of submission. This had no impact on the peer review process and the final decision.

Generative AI statement

The author(s) declare that no Generative AI was used in the creation of this manuscript.

Publisher's note

Supplementary material

The Supplementary Material for this article can be found online at: https://www.frontiersin.org/articles/10.3389/feart.2025.1550746/full#supplementary-material

References

Alvarez, L. W., Alvarez, W., Asaro, F., and Michel, H. V. (1980). Extraterrestrial cause for the cretaceous–tertiary extinction. *Science* 208, 1095–1108. doi:10.1126/science.208.4448.1095

Alvarez, W., Claeys, P., and Kieffer, S. (1995). Emplacement of Cretaceous-Tertiary boundary shocked quartz from Chicxulub crater. *Science* 269, 930–935. doi:10.1126/science.269.5226.930

Arenillas, I., Arz, J. A., Grajales-Nishimura, J. M., Murillo-Muñetón, G., Alvarez, W., Camargo-Zanoguera, A., et al. (2006). Chicxulub impact event is Cretaceous/Paleogene boundary in age: new micropaleontological evidence. *Earth Planet. Sci. Lett.* 249 (3-4), 241–257. doi:10.1016/j.epsl.2006.07.020

Arz, J. A., Alegret, L., and Arenillas, I. (2004). Foraminiferal biostratigraphy and paleoenvironmental reconstruction at Yaxcopoil-1 drill hole,

Chicxulub crater, Yucatan Peninsula. *Meteorit. Planet. Sci.* 39, 1099–1112. doi:10.1111/j.1945-5100.2004.tb01131.x

Arz, J. A., Arenillas, I., Grajales-Nishimura, J. M., Liesa, C. L., Soria, A. R., Rojas, R., et al. (2022). "No evidence of multiple impact scenario across the Cretaceous/Paleogene boundary based on planktic foraminiferal biochronology," in *From the guajira desert to the apennines, and from mediterranean microplates to the Mexican killer asteroid: honoring the career of walter Alvarez*. Editors C. Koeberl, P. Claeys, and A. Montanari (Colorado, CO: Geological Society of America Boulder), 557, 415–448. doi:10.1130/2022.2557(20)

Barton, P. J., Grieve, R. A. F., Morgan, J. V., Surendra, A. T., Vermeesch, P. M., Christeson, G. L., et al. (2010). "Seismic images of Chicxulub impact melt sheet and comparison with the Sudbury structure," in *Large meteorite impacts and planetary evolution IV*. Editors R. L. Gibson, and W. U. Reimold, 465, 103–113.

Batista, J., Pérez-Flores, M. A., and Urrutia-Fucugauchi, J. (2013). Three-dimensional gravity modeling of Chicxulub crater structure, constrained with marine seismic data and land boreholes. *Earth Planets Space* 65, 973–983. doi:10.5047/eps.2013.05.015

Bell, C., Morgan, J., Hampson, G. J., and Trudgill, B. (2004). Stratigraphic and sedimentological observations from seismic data across the Chicxulub impact basin. *Meteorit. Planet. Sci.* 39, 1089–1098. doi:10.1111/j.1945-5100.2004.tb01130.x

Boyce, J. M., and Mouginis-Mark, P. J. (2006). Martian craters viewed by the thermal emission imaging system instrument: double-layered ejecta craters. *J. Geophys. Res. Planets* 111, E10005. doi:10.1029/2005JE002638

Chopra, S., and Marfurt, K. J. (2005). Seismic attributes – a historical perspective. *Geophysics* 70, 3SO–28SO. doi:10.1190/1.2098670

Chopra, S., and Marfurt, K. J. (2008). Emerging and future trends in seismic attributes. *Lead. Edge* 27, 298–318. doi:10.1190/1.2896620

Christeson, G. L., Gulick, S., Morgan, J., Gebhardt, C., Kring, D., Le Ber, E., et al. (2018). Extraordinary rocks from the peak ring of the Chicxulub impact crater: P-wave velocity, density and porosity measurements from IODP/ICDP Expedition 364. *Earth Planet. Sci. Lett.* 495, 1–11. doi:10.1016/j.epsl.2018.05.013

Christeson, G. L., Morgan, J. V., and Gulick, S. P. S. (2021). Mapping the Chicxulub impact stratigraphy and peak ring using drilling and seismic data. *J. Geophys. Res. Planets* 126, e2021JE006938. doi:10.1029/2021JE006938

Christeson, G. L., Nakamura, Y., Buffler, R. T., Morgan, J., and Warner, M. (2001). Deep crustal structure of the Chicxulub impact crater. *J. Geophys. Res.* 106 (21), 21751–21769. doi:10.1029/2001JB000337

Claeys, P., Heuschkel, S., Lounejeva-Baturina, E., Sanchez-Rubio, G., and Stöffler, D. (2003). The suevite of drillhole Yucatán 6 in the Chicxulub impact crater. *Meteorit. Planet. Sci.* 38, 1299–1320. doi:10.1111/j.1945-5100.2003.tb00315.x

Claeys, P., Kiessling, W., and Alvarez, W. (2002). "Distribution of Chicxulub ejecta at the cretaceous-tertiary boundary," in *Catastrophic events and mass extinctions: impacts and beyond*. Editors C. Koeberl, and K. G. MacLeod (Colorado, CO: Geological Society of America Boulder), 356, 55–68.

Collins, G. S., Morgan, J., Barton, P., Christeson, G. L., Gulick, S., Urrutia-Fucugauchi, J., et al. (2008). Dynamic modeling suggests terrace zone asymmetry in the Chicxulub crater is caused by target heterogeneity. *Earth Planet. Sci. Lett.* 270, 221–230. doi:10.1016/j.epsl.2008.03.032

Collins, G. S., Patel, N., Davison, T. M., Rae, A. S., Morgan, J. V., Gulick, S., et al. (2020). A steeply-inclined trajectory for the Chicxulub impact. *Nat. Comm.* 11 (1), 1480. doi:10.1038/s41467-020-15269-x

Connors, M., Hildebrand, A. R., Pilkington, M., Ortíz, C., Chávez, R.U.-F., Graniel-Castro, J., et al. (1996). Yucatan karst features and the size of Chicxulub crater. *Geophys. J. Inter.* 127, F11–F14. doi:10.1111/j.1365-246X.1996.tb04066.x

Cornejo-Toledo, A., and Hernandez-Osuna, A. (1950). Las anomalias gravimetricas en la Cuenca Salina del istmo, Planicie Costera de Tabasco, Campeche y Peninsula de Yucatan. Bol. Asoc. Mex. *Geol. Petrol.* 2, 453–460.

Dasgupta, R., and Clark, R. A. (1998). Estimation of Q from Surface seismic reflection data. *Geophysics* 63, 2120–2128. doi:10.1190/1.1444505

Duong, T. N. M., Hernawan, B., Medina-Zetina, Z., and Urrutia-Fucugauchi, J. (2023). Numerical modeling of an asteroid impact on Earth: matching field observations at the Chicxulub crater using the distinct element method (DEM). *Geosciences* 13 (5), 139. doi:10.3390/geosciences13050139

Escobar-Sánchez, J. E., and Urrutia-Fucugauchi, J. (2010). Chicxulub crater post-impact hydrothermal activity - evidence from Paleocene carbonates in the Santa Elena borehole. *Geofis. Intern.* 49, 97–106. doi:10.22201/igeof.00167169p.2010.49.2.117

Feignon, J.-G., Schulz, T., Ferriere, L., Goderis, S., de Graaff, S., Kaskes, P., et al. (2022). Search for a meteoritic component within the impact melt rocks of the Chicxulub impact structure peak ring, Mexico. *Geochim. Cosmochim. Acta* 323, 74–101. doi:10.1016/j.gca.2022.02.006

French, C. D., and Schenk, C. J. (2004). Map showing geology, oil and gas fields, and geologic provinces of the Caribbean region. *U. S. Geol. Surv. Open-File Rep. 97-470-K, CD-ROM*. doi:10.3133/ofr97470K

Gelinas, A., Kring, D. A., Zurcher, L., Urrutia-Fucugauchi, J., Morton, O., and Walker, R. J. (2004). Osmium isotope constraints on the proportion of bolide component in Chicxulub impact melt rocks. *Meteorit. Planet. Sci.* 39, 1003–1008. doi:10.1111/j.1945-5100.2004.tb00941.x

Goto, K., Tada, R., Tajika, E., Bralower, T., Hasegawa, T., and Matsui, T. (2004). Evidence for ocean water invasion into the Chicxulub crater at the Cretaceous/Tertiary boundary. *Meteorit. Planet. Sci.* 39, 1233–1247. doi:10.1111/j.1945-5100.2004.tb01139.x

Gradstein, F. M., Ogg, J. G., Schmitz, M., and Ogg, G. (2012). *The geologic time scale 2012*. Boston: Elsevier Science Ltd., 1–1144.

Gulick, S., Barton, P., Christeson, G., Morgan, J., MacDonald, M., Mendoza, K., et al. (2008). Importance of pre-impact crustal structure for the asymmetry of the Chicxulub impact crater. *Nat. Geosci.* 1, 131–135. doi:10.1038/ngeo103

Gulick, S., Morgan, J., Mellett, C. L., Green, S. L., Bralower, T., Chenot, E., et al. (2017). "Site M0077: post impact sedimentary rocks," in *Proceed. Intern. Ocean Discovery progr*. Editors J. Morgan, S. Gulick, C. L. Mellett, and S. L. Green, 364, 1–35.

Gulick, S. P. S., Christeson, G. L., Barton, P. J., Grieve, R., Morgan, J., and Urrutia-Fucugauchi, J. (2013). Geophysical characterization of the Chicxulub impact crater. *Rev. Geophys.* 51, 31–52. doi:10.1002/rog.20007

Hildebrand, A. R., Penfield, G. T., Kring, G. T., Pilkington, D. A., Camargo-Zanoguera, M., Jacobsen, A., et al. (1991). Chicxulub Crater: a possible cretaceous/tertiary boundary impact crater on the yucatan peninsula, Mexico. *Geology* 19, 867–871. doi:10.1130/0091-7613(1991)019<0867:CCAPCT>2.3.CO;2

Hildebrand, A. R., Pilkington, M., Ortiz-Aleman, C., Chavez, R. E., Urrutia-Fucugauchi, J., Connors, M., et al. (1998). "Mapping Chicxulub crater structure with gravity and seismic reflection data," Editors M. M. Grady, R. Hutchinson, G. J. H. McCall, and D. A. Rotherby (Geol. Soc., London: Sp. Publ.), 140, 155–176.

Horz, F., Ostertag, R., and Rainey, D. A. (1983). Bunte breccia of the Ries: continuous deposits of large impact craters. *Rev. Geophys. Space Phys.* 21, 1667–1725. doi:10.1029/RG021i008p01667

Kamo, S. L., and Krogh, T. E. (1995). Chicxulub crater source for shocked zircon crystals from the Cretaceous/Tertiary boundary layer, Saskatchewan: evidence from new U-Pb data. *Geology* 23, 281–284. doi:10.1130/0091-7613(1995)023<0281:CCSFSZ>2.3.CO;2

Kamo, S. L., Lana, C., and Morgan, J. V. (2011). U-Pb ages of shocked zircon grains link distal K-Pg boundary sites in Spain and Italy with the Chicxulub impact. *Earth Planet. Sci. Lett.* 310, 401–408. doi:10.1016/j.epsl.2011.08.031

Keller, G., Adatte, T., Stinnesbeck, W., Rebolledo-Vieyra, M., Urrutia-Fucugauchi, J., Kramar, U., et al. (2004). Chicxulub impact predates the K-T boundary mass extinction. *Proceed. Nat. Acad. Sci.* 101, 3753–3758. doi:10.1073/pnas.0400396101

Keppie, D., Dostal, J., Norman, M., Urrutia-Fucugauchi, J., and Grajales-Nishimura, M. (2011). Study of melt and a clast of 546 Ma magmatic arc rocks in the 65 Ma Chicxulub bolide breccia, northern Maya block, Mexico: western limit of Ediacaran arc peripheral to northern Gondwana. *Intern. Geol. Rev.* 53, 1180–1193. doi:10.1080/00206810903545527

Kettrup, B., Deutsch, A., Ostermann, M., and Agrinier, P. (2000). Chicxulub impactites: geochemical clues to the precursor rocks. *Meteorit. Planet. Sci.* 35 (6), 1229–1238. doi:10.1111/j.1945-5100.2000.tb01511.x

Koeberl, C., Sharpton, V., Schuraytz, C., Shirey, S. B., Blum, J. D., and Marin, L. (1994). Evidence for a meteoritic component in impact melt rock from the Chicxulub structure. *Geochem. Cosmochim. Acta* 58, 1679–1684. doi:10.1016/0016-7037(94)90567-3

Kring, D. A. (1995). The dimensions of the Chicxulub impact crater and impact melt sheet. *J. Geophys. Res.* 100 (16), 16979–16986. doi:10.1029/95JE01768

Kring, D. A., and Boynton, W. V. (1992). Petrogenesis of an augite-bearing melt rock in the Chicxulub structure and its relationship to K/T impact spherules in Haiti. *Nature* 358, 141–144. doi:10.1038/358141a0

Kring, D. A., Hörz, L., Zurcher, L., and Urrutia-Fucugauchi, J. (2004). Impact lithologies and their emplacement in the Chicxulub impact crater: initial results from the Chicxulub scientific drilling project, Yaxcopoil, Mexico. *Meteorit. Planet. Sci.* 39, 879–897. doi:10.1111/j.1945-5100.2004.tb00936.x

Krogh, T. E., Kamo, S. L., Bohor, B. F., Marin, L. E., and Hildebrands, A. R. (1993). U-Pb ages of single shocked zircons linking distal K-T ejecta to the Chicxulub crater. *Nature* 366, 731–734. doi:10.1038/366731a0

Kuiper, K. F., Deino, A., Hilgen, F. J., Krijsman, W., Renne, P. R., and Wijbrans, J. R. (2008). Synchronizing rock clocks of Earth history. *Science* 320, 500–504. doi:10.1126/science.1154339

Kumar, P., and Foufoula-Georgiou, E. (1997). Wavelet analysis for geophysical applications. *Rev. Geophys.* 35, 305–402. doi:10.1029/97RG00427

Limon, L., and Baron, L. (1954). Informe del estudio micropaleontologico del pozo Chicxulub No. 1. Petroleos Mexicanos, Gerencia de Exploracion. *Lab. Paleontol. Petrogr. Inf. No. LPP-8*.

Lopez Ramos, E. (1975). "Geological summary of the Yucatan peninsula," in *The Ocean basins and margins, vol. 3, the Gulf of Mexico and the caribbean*. Editors A. E. M. Nairn, and F. G. Stehli (New York: Plenum), 257–282.

López Ramos, E. (1983). *Geología de México*, 3. México: Tomo, 445.

Marín, L. E., Sharpton, V. L., Urrutia Fucugauchi, J., Sikora, P., and Carney, C. (1994). The "Upper Cretaceous Unit" in the Chicxulub multiring basin: new age based on

planktic foraminiferal assemblage. *New Dev. regarding KT event other catastrophes Earth Hist. Houst. Tex. Lunar Planet* 825, 77.

Marín, L. E., Sharpton, V. L., Urrutia-Fucugauchi, J., Smit, J., Sikora, P., Carney, C., et al. (2001). Stratigraphy at ground zero: a contemporary evaluation of well data in the Chicxulub impact basin. *Intern. Geol. Rev.* 43, 1143–1149. doi:10.1080/00206810109465066

Melosh, H. J. (1989). *Impact cratering: a geologic process*. New York: Oxford University Press, 245.

Melosh, H. J., and Ivanov, B. A. (1999). Impact crater collapse. *Ann. Rev. Earth Planet. Sci.* 27 (1), 385–415. doi:10.1146/annurev.earth.27.1.385

Meyerhoff, A. A., Lyons, J. B., and Officer, C. B. (1994). Chicxulub structure: a volcanic sequence of Late Cretaceous age. *Geology* 22 (1), 3–4. doi:10.1130/0091-7613(1994)022<0003:csavso>2.3.co;2

Molina, E., Alegret, L., Arenillas, I., Arz, J. A., Gallala, N., Hardenbol, J., et al. (2006). The global boundary stratotype section and point for the base of the Danian stage (Paleocene, Paleogene, "Tertiary," Cenozoic) at El Kef, Tunisia - original definition and revision. *Episodes* 29 (4), 263–273. doi:10.18814/epiiugs/2006/v29i4/004

Molina-Garza, R. S., Van der Voo, R., and Urrutia-Fucugauchi, J. (1992). Paleomagnetism of the Chiapas massif, southern Mexico: evidence for rotation of the Maya block and implications for the opening of the Gulf of Mexico. *Geol. Soc.Am. Bul.* 104 (9), 1156–1168. doi:10.1130/0016-7606(1992)104<1156:potcms>2.3.co;2

Morgan, J., Gulick, S., Bralower, T., Chenot, E., Christeson, G., Claeys, P., et al. (2016). The formation of peak rings in large impact craters. *Science* 354, 878–882. doi:10.1126/science.aah6561

Morgan, J., Gulick, S., Mellet, C. L., Green, S. L., and Expedition 364 Scientists (2017). Chicxulub: drilling the K-Pg impact crater. *Proc. Int. Ocean. Discov. Program* 364. doi:10.14379/iodp.proc.364.2017

Morgan, J., Warner, M., Chicxulub group, Brittan, J., Buffler, R., Camargo, A., et al. (1997). Size and morphology of the Chicxulub impact crater. *Nature* 390, 472–476. doi:10.1038/37291

Morgan, J., Warner, M., Collins, G. S., Melosh, H. J., and Christeson, G. L. (2000). Peak-ring formation in large impact craters: geophysical constraints from Chicxulub. *Earth Planet. Sci. Lett.* 183, 347–354. doi:10.1016/S0012-821X(00)00307-1

Morgan, J. V., Lana, C., Kearsley, A., Coles, B., Belcher, C., Montanari, S., et al. (2006). Analyses of shocked quartz at the global K-P boundary indicate an origin from a single, high-angle, oblique impact at Chicxulub. *Earth Planet. Sci. Lett.* 251, 264–279. doi:10.1016/j.epsl.2006.09.009

Morgan, J. V., Warner, M., Urrutia-Fucugauchi, J., Gulick, S., Christeson, G., Barton, P., et al. (2005). Chicxulub crater seismic survey prepares way for future drilling. *EOS Trans. Am. Geophys. Union* 86, 325–332. doi:10.1029/2005EO360001

Ortiz-Aleman, C., and Urrutia-Fucugauchi, J. (2010). Aeromagnetic anomaly modeling of central zone structure and magnetic sources in the Chicxulub crater. *Phys. Earth Planet. Inter.* 179, 127–138. doi:10.1016/j.pepi.2010.01.007

Pan, S., Hsieh, B., Lu, M., and Lin, Z. (2008). Identification of stratigraphic formation interfaces using wavelet and Fourier transforms. *Comput. Geosci.* 34, 77–92. doi:10.1016/j.cageo.2007.01.002

Penfield, G. T., and Camargo-Zanoguera, A. (1981). "Definition of a major igneous zone in the central Yucatán platform with aeromagnetics and gravity," in *Technical program, abstracts, 51st annual meeting* (Tulsa, Oklahoma: Soc. Expl. Geophys.), 37.

Pérez-Cruz, L., and Urrutia-Fucugauchi, J. (2024). Chicxulub´s legacy: breakthroughs from scientific drilling, tsunamis, global climate upheaval and mass extinction. *Past. Glob. Chang. Mag.* 32 (2), 82–83. doi:10.22498/pages.32.2.82

Pérez-Drago, G., Gutierrez, A., Pérez-Cruz, L., and Urrutia-Fucugauchi, J. (2008). *Chicxulub impact crater and Yucatan carbonate platform – PEMEX oil exploration*. Washington, DC: American Geophysical Union. V53A-2141 abstract.

Petroleos Mexicanos (1953). *Reporte final del pozo Chicxulub-1. Gerencia de Exploración*. México: Petróleos Mexicanos.

Petroleos Mexicanos (1955). *Reporte final del pozo Sacapuc-1. Gerencia de Exploración*. México: Petróleos Mexicanos.

Petroleos Mexicanos (1967). *Reporte final del pozo Yucatan-6. Gerencia de Exploración*. México: Petróleos Mexicanos.

Pierazzo, E., and Melosh, H. J. (2000). Understanding oblique impacts from experiments, observations, and modeling. *Ann. Rev. Earth Planet. Sci.* 28, 141–167. doi:10.1146/annurev.earth.28.1.141

Pilkington, M., and Hildebrand, A. R. (2000). Three-dimensional magnetic imaging of the Chicxulub crater. *J. Geophys. Res.* 105, 23479–23491. doi:10.1029/2000JB900222

Pilkington, M., Hildebrand, A. R., and Ortiz-Aleman, C. (1994). Gravity and magnetic field modeling and structure of the Chicxulub crater, Mexico. *J. Geophys. Res.* 99, 147–162. doi:10.1029/94JE01089

Pindell, J. L., and Dewey, J. F. (1982). Permo-Triassic reconstruction of western Pangea and the evolution of the Gulf of Mexico/Caribbean region. *Tectonics* 1, 197–211. doi:10.1029/TC001i002p00179

Pope, K., Ocampo, A. C., Fisher, A. G., Vega, F., Ames, D. E., King, D. T., et al. (2005). Chicxulub impact ejecta deposits in southern Quintana Roo, Mexico, and central Belize. *Geol. Soc. Am. Sp. Pap.* 384, 171–190. doi:10.1130/0-8137-2384-1.171

Rae, A. S., Collins, G. S., Morgan, J. V., Salge, T., Christeson, G. L., Leung, J., et al. (2019). Impact-induced porosity and microfracturing at the Chicxulub impact structure. *J. Geophys. Res.Journal Geophys. Res. Planets* 124 (7), 1960–1978. doi:10.1029/2019JE005929

Ramirez-Cruz, L., del Valle-Garcia, R., and Urrutia-Fucugauchi, J. (2005). Enhanced oil production in a mature field assisted by spectral attenuation analysis. *J. Geophys. Eng.* 2, 48–53. doi:10.1088/1742-2132/2/1/007

Rebolledo-Vieyra, M., and Urrutia-Fucugauchi, J. (2006). Magnetostratigraphy of the Cretaceous/Tertiary boundary and early Paleocene sedimentary sequence from the Chicxulub impact crater. *Earth Planets Space* 58, 1309–1314. doi:10.1186/BF03352626

Riller, U., Pölchau, M., Rae, A., Schulte, F., Collins, G., Melosh, J., et al. (2018). Rock fluidization during peak-ring formation of large impact structures. *Nature* 562 (7728), 511–518. doi:10.1038/s41586-018-0607-z

Salguero-Hernández, E., Pérez-Cruz, L., and Urrutia-Fucugauchi, J. (2020). Seismic attribute analysis of Chicxulub impact crater. *Acta geophys.* 68 (3), 627–640. doi:10.1007/s11600-020-00442-z

Salguero-Hernández, E., Urrutia-Fucugauchi, J., and Ramírez-Cruz, L. (2010). Fracturing and deformation in the Chicxulub crater - complex trace analysis of instantaneous seismic attributes. *Rev. Mex. Ciencias Geol.* 27 (1), 175–184.

Schmieder, M., Shaulis, B. J., Lapen, T. J., and Kring, D. A. (2018). U–Th–Pb systematics in zircon and apatite from the Chicxulub impact crater, Yucatan, Mexico. *Mag* 155 (6), 1330–1350. doi:10.1017/S0016756817000255

Schmitt, R. T., Wittmann, A., and Stöffler, D. (2004). Geochemistry of drill core samples from Yaxcopoil-1, Chicxulub impact crater, Mexico. *Meteorit. Planet. Sci.* 39, 979–1001. doi:10.1111/j.1945-5100.2004.tb00940.x

Schulte, P., Alegret, L., Arenilla, I., Arz, J. A., Barton, P. J., Bown, P. R., et al. (2010). The Chicxulub asteroid impact and mass extinction at the Cretaceous-Paleogene boundary. *Science* 327, 1214–1218. doi:10.1126/science.1177265

Schuraytz, B. C., Lindstrom, D. J., Marin, L., Martinez, R. R., Mittlefehldt, D. W., Sharpton, V., et al. (1996). Iridium metal in Chicxulub impact melt: forensic chemistry on the K-T smoking gun. *Science* 271, 1573–1576. doi:10.1126/science.271.5255.1573

Schuraytz, B. C., Sharpton, V. L., and Marin, L. (1994). Petrology of impact-melt rocks at the Chicxulub multiring basin, Yucatán, Mexico. *Geology* 22, 868–872. doi:10.1130/0091-7613(1994)022<0868:POIMRA>2.3.CO;2

Sharpton, V. L., Burke, K., Camargo-Zanoguera, A., Hall, S. A., Lee, S., Marin, L. E., et al. (1993). Chicxulub multiring impact basin: size and other characteristics derived from gravity analysis. *Science* 261, 1564–1567. doi:10.1126/science.261.5128.1564

Sharpton, V. L., Dalrymple, G. B., Marin, L. E., Ryder, G., Schuraytz, B. C., and J. Urrutia-Fucugauchi, J. (1992). New links between the Chicxulub impact structure and the Cretaceous/Tertiary boundary. *Nature* 359, 819–821. doi:10.1038/359819a0

Simonds, C. H., Floran, R. J., Mcgee, P. E., Phinney, W. C., and Warner, J. L. (1978). Petrogenesis of melt rocks, Manicouagan impact structure, Quebec. *J. Geophys. Res.* 83, 2773–2788. doi:10.1029/JB083iB06p02773

Smit, J., Van der Gaast, S., and Lustenhouwer, W. (2004). Is the transition impact to post-impact rock complete? Some remarks based on XRF scanning, electron microprobe, and thin section analyses of the Yaxcopoil-1 core in the Chicxulub crater. *Meteorit. Planet. Sci.* 39, 1113–1126. doi:10.1111/j.1945-5100.2004.tb01132.x

Stöffler, D., Artemieva, N. A., Ivanov, B. A., Hecht, L., Kenkmann, T., Schmitt, R. F., et al. (2004). Origin and emplacement of the impact formation at Chicxulub, Mexico as revealed by the ICDP deep drilling at Yaxcopoil-1 and by numerical modeling. *Meteorit. Planet. Sci.* 39, 1035–1067. doi:10.1111/j.1945-5100.2004.tb01128.x

Stöffler, D., Artemieva, N. A., Wünnemann, K., Reimold, W. U., Jacob, J., Hansen, B. K., et al. (2013). Ries crater and suevite revisited—observations and modeling Part I: observations. *Meteorit. and Planet. Sci.* 48 (4), 515–589. doi:10.1111/maps.12086

Sturm, S., Wulf, G., Jung, D., and Kenkmann, T. (2013). The Ries impact, a double-layer rampart crater on Earth. *Geology* 41, 531–534. doi:10.1130/G33934.1

Tagle, R., Erzinger, J., Hecht, L., Schmitt, R. T., Stöffler, D., and Claeys, P. (2004). Platinum group elements in impactites of the ICDP Chicxulub drill core Yaxcopoil-1: are there traces of the projectile? *Meteorit. Planet. Sci.* 39, 1009–1016. doi:10.1111/j.1945-5100.2004.tb00942.x

Taner, M. T., Koehler, F., and Sheriff, R. E. (1979). Complex seismic trace analysis. *Geophysics* 44 (6), 1041–1063. doi:10.1190/1.1440994

Timms, N. E., Pearce, M. A., Erickson, T. M., Cavosie, A. J., Rae, A. S. P., Wheeler, J., et al. (2019). New shock microstructures in titanite ($CaTiSiO_5$) from the peak ring of the Chicxulub impact structure, Mexico. *Contrib. Mineral. Petrol.* 174, 38. doi:10.1007/s00410-019-1565-7

Tuchscherer, M. G., Reimold, W. U., Koeberl, C., and Gibson, R. L. (2004). Major and trace element characteristics of impactites from the Yaxcopoil-1 borehole, Chicxulub structure, Mexico. *Meteorit. Planet. Sci.* 39, 955–978. doi:10.1111/j.1945-5100.2004.tb00939.x

Urrutia-Fucugauchi, J., Arellano-Catalán, O., Pérez-Cruz, L., and Romero-Galindo, I. A. (2022). Chicxulub crater joint gravity and magnetic anomaly analysis: structure,

asymmetries, impact trajectory and target structures. *Pure Appl. Geophys.* 179 (8), 2735–2756. doi:10.1007/s00024-022-03074-0

Urrutia-Fucugauchi, J., Camargo-Zanoguera, A., Pérez-Cruz, L., and Pérez-Cruz, G. (2011). The Chicxulub multi-ring impact crater, Yucatan carbonate platform, Gulf of Mexico. *Geofis. Intern.* 50, 99–127. doi:10.22201/igeof.00167169p.2011.50.1.125

Urrutia-Fucugauchi, J., Chavez, J. M., Pérez-Cruz, L., and de la Rosa, J. L. (2008). Impact ejecta and carbonate sequence in the eastern sector of Chicxulub Crater. *Comptes Rendus Geosci.* 340, 801–810. doi:10.1016/j.crte.2008.09.001

Urrutia-Fucugauchi, J., Marin, L., and Sharpton, V. L. (1994). Reverse polarity magnetized melt rocks from the Cretaceous/Tertiary Chicxulub structure, Yucatan peninsula, Mexico. *Tectonophysics* 237, 105–112. doi:10.1016/0040-1951(94)90161-9

Urrutia-Fucugauchi, J., Marin, L., and Trejo, A. (1996). UNAM scientific drilling program of Chicxulub impact structure – evidence for a 300 kilometer crater diameter. *Geophys. Res. Lett.* 23, 1565–1568. doi:10.1029/96GL01566

Urrutia-Fucugauchi, J., Morgan, J., Stoeffler, D., and Claeys, P. (2004). The Chicxulub scientific drilling project (CSDP). *Meteorit. Planet. Sci.* 39, 787–790. doi:10.1111/j.1945-5100.2004.tb00928.x

Urrutia-Fucugauchi, J., and Pérez-Cruz, L. (2008). Post-impact carbonate deposition in the Chicxulub impact crater region, Yucatan platform, Mexico. *Curr. Sci.* 95, 248–252. Available online at: https://www.jstor.org/stable/24103055.

Urrutia-Fucugauchi, J., and Pérez-Cruz, L. (2009). Multiring-forming large bolide impacts and evolution of planetary surfaces. *Int. Geol. Rev.* 51, 1079–1102. doi:10.1080/00206810902867161

Urrutia-Fucugauchi, J., Pérez-Cruz, L., Campos, S. E., Escobar, J. E., and Velasco-Villarreal, M. (2014). Magnetic susceptibility logging of Chicxulub proximal impact breccias in the Santa Elena borehole – implications for emplacement mode. *Std. Geophys. Geod.* 58, 100–120. doi:10.1007/s11200-013-0803-0

Urrutia-Fucugauchi, J., Pérez-Cruz, L., Venegas-Ferrer, R., and Sánchez-Solís, P. (2025). The Chicxulub crater drilling program-borehole core characterization, scanning and logging: Chicxulub drilling program. *Geol. Acta* 23, 1–21. doi:10.1344/GeologicaActa2025.23.3

Vermeesch, P. M., and Morgan, J. V. (2008). Structural uplift beneath the Chicxulub impact structure. *J. Geophys, Res.* 113 (B7), B07103. doi:10.1029/2007JB005393

Vermeesch, P. M., Morgan, J. V., Christeson, G. L., Barton, P. J., and Surendra, A. (2009). Three-dimensional joint inversion of traveltime and gravity data across the Chicxulub impact crater. *J. Geophys. Res.* 114, BO2105. doi:10.1029/2008JB005776

Ward, W., Keller, G., Stinnesbeck, W., and Adatte, T. (1995). Yucatan subsurface stratigraphy Implications and constraints for the Chicxulub impact. *Geology* 23, 873–876. doi:10.1130/0091-7613(1995)023<0873:YNSSIA>2.3.CO;2

Warren, P. H., Claeys, P., and Cedillo-Pardo, E. (1996). "Mega-impact melt petrology (Chicxulub, Sudbury, and the Moon): effects of scale and other factors on potential for fractional crystallization and development of cumulates," in *The cretaceous-tertiary event and other catastrophes in earth history*. Editors G. Ryder, D. Fastovsky, and S. Gartner (Boulder, Colorado: Geological Society of America Special). Paper 307.

Whalen, M., Gulick, S., Pearson, Z., Norris, R. D., Pérez-Cruz, L., and Urrutia-Fucugauchi, J. (2014). Annealing the Chicxulub impact: Paleogene Yucatan carbonate slope development in the Chicxulub impact basin, Mexico. *Soc. Sed. Geol. Sp. Publ.* 105, 282–304. doi:10.2110/sepmsp.105.04

Whalen, M. T., Gulick, S. P., Lowery, C. M., Bralower, T. J., Morgan, J. V., Grice, K., et al. (2020). Winding down the Chicxulub impact: the transition between impact and normal marine sedimentation near ground zero. *Mar. Geol.* 430, 106368. doi:10.1016/j.margeo.2020.106368

Wittmann, A., Cavosie, A. J., Timms, N. E., Ferrière, L., Rae, A., Rasmussen, C., et al. (2021). Shock impedance amplified impact deformation of zircon in granitic rocks from the Chicxulub impact crater. *Earth Planet. Sci. Lett.* 575, 117201. doi:10.1016/j.epsl.2021.117201

Wittmann, A., Kenkmann, T., Hecht, L., and Stöffler, D. (2007). Reconstruction of the Chicxulub ejecta plume from its deposits in drill core Yaxcopoil-1. *Geol. Soc. Am. Bull.* 119, 1151–1167. doi:10.1130/B26116.1

Zhao, J., Xiao, L., Gulick, S. P., Morgan, J. V., Kring, D., Urrutia-Fucugauchi, J., et al. (2020). Geochemistry, geochronology and petrogenesis of Maya Block granitoids and dykes from the Chicxulub impact crater, Gulf of Mexico: implications for the assembly of Pangea. *Gondwana Res.* 82, 128–150. doi:10.1016/j.gr.2019.12.003